*J. Fluid Mech.* (1984), *vol.* 145, *pp.* 305–337
*Printed in Great Britain*



# Large-scale structural effects in developed turbulent flow through closely-spaced rod arrays

By J. D. HOOPER

CSIRO, Division of Mineral Physics, Lucas Heights Research Establishment, Private Mail Bag 7, P.O. Sutherland, NSW 2232, Australia

AND K. REHME

Institut für Neutronenphysik und Reaktortechnik, Kernforschungszentrum Karlsruhe, Postfach 3640, D7500 Karlsruhe 1, W. Germany

(Received 3 November 1983)

Axial and azimuthal turbulence intensities in the rod-gap region are shown, for developed turbulent flow through parallel rod arrays, to increase strongly with decreasing rod spacing. Two array geometries are reported: one was constructed from a rectangular cross-section duct containing four rods and spaced at five pitch-to-diameter or wall-to-diameter ratios; the second was a test section containing six rods set in a regular square-pitch array to represent the interior flow region of a large array.

Measurements were made of the mean axial velocity, wall-shear-stress variation, axial-pressure distribution and Reynolds stresses. Techniques for resolving secondary-flow velocities to within $\pm 1\,\%$ of the local axial velocity failed to detect significant non-zero mean secondary-flow components. Analysis of the turbulent flow structure showed an energetic azimuthal turbulent-velocity component in the open rod gap for both geometries. The axial turbulent velocity has a coupled large-scale semiperiodic structure, with an antiphase relationship across the rod-gap centre or subchannel boundary. This structure is considered to be generated by an incompressible-flow parallel-channel instability, and, for closely spaced rod arrays, is the dominant process for intersubchannel mass, heat or momentum exchange.

## 1. Introduction

The structure of axially developed turbulent flow through large regularly spaced rod arrays is of considerable importance to the design and analysis of the thermo-hydraulics of nuclear power-reactor cores. This flow is fundamental to the core-coolant fluid dynamics of most reactor systems. Of particular significance are features that promote intersubchannel heat and momentum transfer, and thereby reduce the azimuthal variation of both the wall-shear-stress distribution and local heat-transfer coefficient. In this paper we demonstrate the presence of a very energetic turbulent intersubchannel momentum-exchange process in the flow through very closely spaced open rod arrays. This process is inadequately described by the accepted mean-axial-vorticity $\Omega_z$ or mean secondary flow ($V$, $W$) model. Other experimental studies are reviewed to place this finding within the context of contemporary data.

Experimental rigs and techniques are described in §2; full details of the hot-wire anemometry and other techniques employed by each author are available upon request. The most significant results of the independent studies are summarized in §§3 and 4, where the amplification of certain components of the Reynolds stresses

is shown to be systematically dependent on the decreasing rod gap width; full details of the experimental results (mean flow, wall shear stress and Reynolds-stress distribution) are also available upon request. In §5 a joint study is given of the turbulent fluid structure in the rod-gap region for both rigs, and experimental evidence presented for an incompressible-flow parallel-channel instability.

Gross or subchannel-averaged mixing experiments have demonstrated that turbulent diffusion between adjacent subchannels is generally higher than that predicted by isotropic diffusion theory. It is also relatively independent of the rod-gap width $g$ or rod pitch-to-diameter $p/d$ ratio for a wide range of rod spacings (Galbraith & Knudsen 1972).

The most likely transport process, for developed single-phase turbulent flow and internal to each subchannel, has been considered to be the generation of an axial mean-vorticity component. The principal production term for this component (Brundrett & Baines 1964; Perkins 1970) is the azimuthal and radial gradient of the two normal Reynolds-stress components acting in the plane normal to the duct axis. The resultant non-axial mean-velocity components $V$ and $W$ circulate in cells bounded by the symmetry axes of the duct cross-section. Considerable experimental data are available for the Reynolds-stress distribution, magnitude and location of such secondary-flow cells for developed flow through square ducts or corners. The early results of Brundrett & Baines (1964) have been confirmed by Perkins (1970), Launder & Ying (1972), Gessner (1973) and Melling & Whitelaw (1976).

Aly, Trupp & Gerrard (1978) have shown that an equilateral triangular cross-section duct has similar pairs of counter-rotating secondary-flow cells in each duct corner. This geometry was chosen to represent the subchannels formed by a triangular pitch rod array spaced at a $p/d$ ratio of 1. Aly *et al.* found that the distribution of the principal or normal components of the Reynolds stresses, normal to the duct wall, was similar to those established for developed axisymmetric pipe flow or two-dimensional boundary-layer flow. The maximum level of the mean secondary flow was approximately 1.5% of the bulk axial velocity. Secondary-flow cells within a symmetrical open rod array are bounded by the same symmetry requirements as the square or equilateral-triangle cross-section duct, and may not cross the subchannel boundary at the centre of the rod gap. However, by transporting higher-momentum fluid from the subchannel centre to the rod-gap area, such cells reduce the azimuthal variation of the wall shear stress. Aly *et al.* gave one extreme limit ($p/d = 1$) for the possible rod spacings in regular triangular arrays, with the wall-shear-stress variation decreasing as the $p/d$ ratio increased. If, when scaled by the local wall shear stress, the distribution of the normal Reynolds stress components normal to the rod wall is similar to that for axisymmetric pipe flow (e.g. Lawn 1971), then the source term for a mean axial vorticity $\Omega_z$ becomes correspondingly smaller with increasing $p/d$ ratio for both triangular- and square-pitch rod arrays.

It is therefore not surprising that the detection of secondary-flow cells in open rod arrays has proved to be difficult. Kjellström (1974) measured the mean-velocity distribution, wall-shear-stress variation and five of the Reynolds stresses in a triangular array with a $p/d$ ratio of 1.217. Secondary-flow components of the order of 1% of the mean axial flow were found by hot-wire anemometry. However, these results indicated a circulation about one rod of the array, an effect attributed either to insufficient flow-development length or to array constructional tolerances. The radial distributions of the three normal Reynolds-stress components were similar to developed axisymmetric pipe flow for each traverse angle, when normalized by the local wall shear stress.

Trupp & Azad (1975) used a triangular array with $p/d$ ratios of 1.50, 1.35 and 1.20 and hot-wire anemometry to determine the distribution of five of the Reynolds stresses. The mean axial-velocity distribution and wall-shear-stress variation were also measured by Pitot and Preston tubes, respectively. Secondary-flow cells were inferred from the wall-shear-stress variation and the turbulent kinetic-energy distribution, without direct resolution by hot-wire anemometry. The radial distribution of the three normal Reynolds stresses was again similar to axisymmetric developed pipe flow. Rowe (1973) used water as the working fluid, and a laser-Doppler anemometer to resolve the mean-velocity distribution and two components of the Reynolds stresses, for developed single-phase flow through a square-pitch array with $p/d$ ratios of 1.250 and 1.125. Multiple secondary-flow cells were proposed for the repeated symmetry zones of the subchannel, based on the distribution of the axial turbulence intensity. The laser-Doppler system could not directly resolve the mean secondary-flow components. In a study of a triangular array with a $p/d$ ratio of 1.123, Carajilescov & Todreas (1976) used the same technique, but failed to measure the mean secondary-flow velocities directly. They concluded, by analysis of the experimental errors, that the mean secondary-flow components were less than 0.67 % of the mean axial velocity.

Seale (1979) measured eddy heat diffusivities in the open rod gap for three $p/d$ ratios in a regularly spaced, single row of rods, enclosed by a long horizontally mounted rectangular duct. Heat transfer was not from the rod surface to the air coolant, but from the heated top wall of the duct to the water-cooled lower wall. The insulated rod walls reduced the rod conduction component to about 2 % of the total heat flow. Seale found that the effective eddy heat diffusivity in the rod gap is strongly anisotropic, and that there is little evidence of secondary flows. In a more recent study on a duct simulating two subchannels of a rod array spaced at a $p/d$ ratio of 1.20, Seale (1982) provided detailed measurements of the mean axial-velocity distribution. Hot-wire anemometry was used to determine the Reynolds-stress distribution, and to resolve successfully secondary-flow cells circulating in the repeated symmetry zones of the duct. Particular emphasis was placed on the maintenance of the dimensional accuracy of the test section, since crossflows created by geometric imperfections of the rig might readily swamp the Reynolds-stress-generated mean secondary flows. The maximum secondary-flow velocities, attained by the cells circulating in the square corners of the duct, were 1.5 % of the bulk axial velocity. These were flows similar to the mean axial vorticity generated in the corners of square-cross-section ducts. The maximum level in the single open rod-gap area was considerably less, being approximately 0.5 % of the bulk axial velocity. Distributions of the principal Reynolds stresses normal to the duct wall were again similar to those observed in axisymmetric pipe or two-dimensional channel flow.

In summary, the experimental studies, including the study of an equilateral triangular duct, have shown that the radial distributions of the normal components of Reynolds stresses are similar to that for developed axisymmetric pipe flow. The radial distribution of the Reynolds shear stress $-\rho\overline{uv}$ for the turbulent core region is effectively a linear function of the wall distance. The azimuthal component of the Reynolds shear stress $-\rho\overline{uw}$ is relatively small for the whole subchannel area, with unresolvable or near-zero levels of the Reynolds shear stress $-\rho\overline{vw}$ acting in the plane normal to the duct axis. Departure from the above generalizations depends to some degree on the array geometry; the wall-shear-stress variation and change in the Reynolds-stress distribution are higher for the square pitch than for the triangular pitch array at equal rod spacings. From the above reviews it appears that there is

a smooth and continuous transition from the turbulent flow structure in regular widely spaced rod arrays, to flow through very closely spaced arrays. Furthermore, in closely spaced rod arrays, it follows that the mean secondary flows driven by the azimuthal and radial gradients of the non-axial Reynolds stresses $-\rho\overline{v^2}$, $-\rho\overline{w^2}$ (Haque *et al.* 1983) should be of greatest magnitude in the rod-gap area.

The experimental studies of Rehme (1977, 1978*a*,*b*, 1980 *a*,*b*,*c*, 1981, 1982*a*,*b*,*c*,*d*), for very closely spaced rod arrays, and Hooper (1980*a*,*b*) are summarized in §§3 and 4 respectively; they show consistently that the mean-axial-vorticity or secondary-flow model is inadequate. The structural study of turbulent flow in the rod gap (§5) indicates an alternative and dominant intersubchannel momentum-exchange process for developed inline flow through closely spaced rod arrays.

## 2. Experimental rigs and measurement technique

Results from the two experimental series of Rehme and Hooper are used. The Rehme rig was a rectangular duct enclosing four rods with a range of $p/d$ and $w/d$ ratios. The second rig consisted of a six-rod cluster set in a square-pitch array to model an interconnected pair of symmetrical interior subchannels with $p/d$ ratios of 1.194 and 1.107.

### 2.1. *Wall-bounded rod array*

The rectangular duct is shown in figure 1, with the geometry of one experiment in the above series. The aluminium tubes were machined to a high surface finish, with a mean roughness depth at the surface of 0.6 μm. The rectangular channel was manufactured from Plexiglas sheets stiffened by ribs, with one of the short walls adjustable to allow changes to the channel geometry. The test-section was 7.0 m in length, and both the channel walls and rods were made up from four 1.750 m sections. Small 2 mm diameter pins were used as rod-gap spacers at four levels in the test-section to maintain the required rig geometry. The working fluid (air) was delivered to the test section through an open honeycomb filter, after prefiltering to remove particles greater than 1 μm.

The ratio of tube diameter to a typical nuclear-fuel-pin diameter is approximately 22.5:1. This scale is large in order to allow a satisfactory spatial resolution of the rod gap for low $p/d$ ratios, using 0.6 mm diameter Pitot tubes and Disa single-wire (normal and 45° inclined) hot-wire anemometer probes.

A microscope with a very short depth of field was used to define the probe position accurately. The microscope was focused sharply onto the end of a pointer, whose absolute position was known in relation to the test section. The pointer was replaced by the probe, which was then brought into sharp focus without altering the microscope setting. The probe position was known to within approximately 5 μm, the microscope depth of field.

Single normal and slant-wire Disa hot-wire anemometer probes (model 55p12 and 55p11) were used to measure the Reynolds stresses, in conjunction with a Disa Model 55M01 constant-temperature anemometer bridge. The slant-wire probe was rotated to the quadrature positions, and each position was corrected to allow for rotational inaccuracy. Positional accuracy is necessary to allow resolution of the very small secondary-flow velocities by the inclined-wire probe, particularly in regions with a high mean-velocity gradient close to the rod wall. The hot-wire probes were statically calibrated before and after use. The nonlinear bridge output signal was used to calculate the Reynolds stresses and the direction of the mean-velocity vector. The slant hot-wire probe correlation is similar to that developed by Champagne & Sleicher

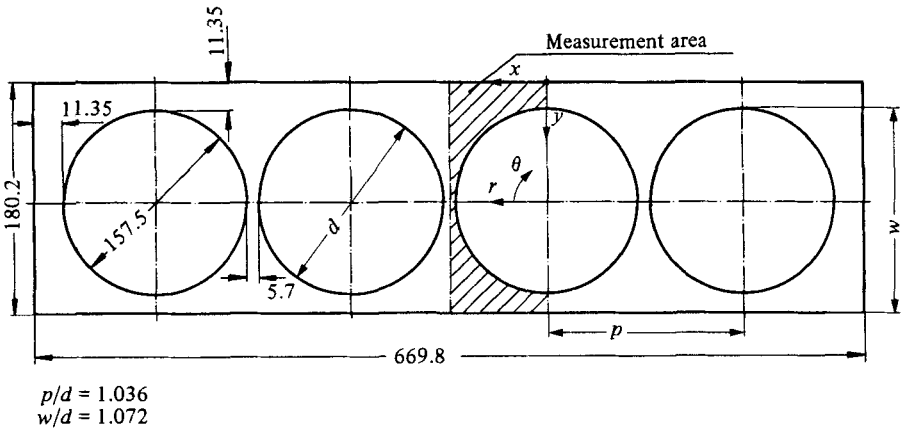


FIGURE 1. Wall-bounded subchannel test section.

(1967), and allows a cooling effect of the velocity component parallel to the wire.

A constant Reynolds number was maintained with a reference pressure from a Pitot probe fixed in a duct corner. The reference pressure was scaled to allow for changes in atmospheric pressure; the second-order effect of humidity on air properties was ignored. The wall-shear-stress distribution was determined by Preston tube, using the correlations of Patel (1965). For full details of the experimental techniques see Rehme (1977).

### 2.2. *Symmetrical square-pitch rod cluster*

The six-rod cluster test section (figure 2) was built to model the fluid mechanics inside a large symmetrical square-pitch rod array. Air was delivered by a centrifugal blower driven by an induction motor, passing into the test section through 15 m of 200 mm diameter ducting and a 1.2 m diameter flow-settling drum fitted internally with a fine mesh screen. The rod diameter was 140 mm and the test-section length 9.14 m, allowing 128 hydraulic diameters for flow development. An external frame supported the rods and the rod-gap walls, and maintained dimensional accuracy without the need for internal spacer pins.

To test the establishment of developed flow conditions at the measurement plane, normally 100 mm from the duct exit, the test-section entry conditions were changed from an open entry to an additional multi-element mesh screen placed immediately outside the duct entrance. The pressure loss at this screen was approximately equal to the pressure drop for the whole test-section length. Since no significant differences were found in either the mean flow structure or of the distribution of the Reynolds stresses (Hooper 1980*a*), it was established that the flow was developed.

All components of the Reynolds stresses, including the Reynolds shear stress $-\rho\overline{vw}$, were measured with a two-element rotating hot-wire anemometer probe. A single inclined wire was located centrally on the probe axis, and a single normal wire was mounted approximately 0.4 mm from the axis. The probe response correlations were developed by Bruun (1976), and the effective inclined-wire angle, determined by a yaw calibration, was used instead of the optically measured angle in the cosine response law. A PDP11/10 computer was used on-line to position the probe in three axes and to measure basic data to preset statistical accuracy limits. The nonlinear bridge output signal of the ISVR (Southampton University) developed hot-wire

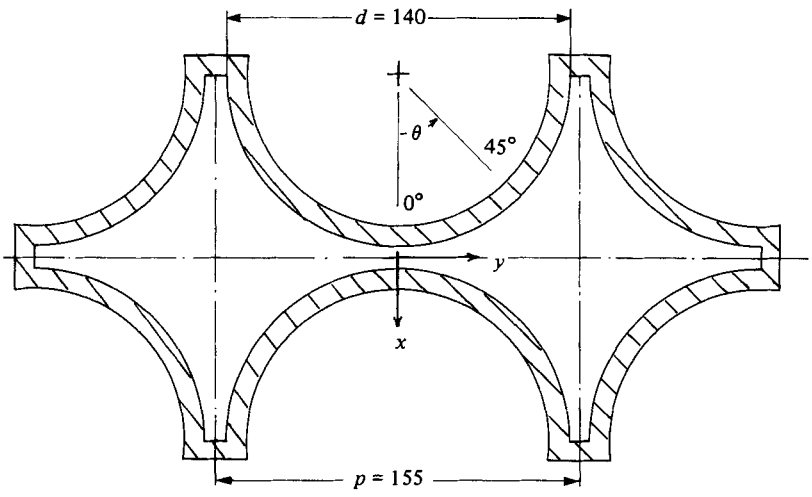


FIGURE 2. Symmetrical square-pitch rod-cluster test section.

anemometers was used to measure the Reynolds stresses. A method of continuously monitoring the steady-state response of the hot-wire probes was described by Hooper (1980*a*), together with further details of the signal processing.

## 3. Experimental results; wall-bounded rod array

The data are selected from the Rehme wall-bounded rod-array experiments to demonstrate, for both the mean and turbulent flow structure, the effect of decreasing the $p/d$ and $w/d$ ratios.

### 3.1. *Wall-shear-stress distribution*

The rod and duct wall-shear-stress variation, for a Reynolds number of $5.46 \times 10^4$ and normalized by the mean of each distribution, is shown in figure 3 for a $p/d$ ratio of 1.071 and a $w/d$ ratio of 1.026 (Rehme 1982*b*). The rod wall shear stress is for a rod-centred cylindrical coordinate system $(r, \theta)$ with the origin for $\theta$ in the centre of the rod-to-rod gap; the Cartesian coordinates $(x, y)$ for the duct wall distribution refer to an $x$-axis origin in the centre of the rod-to-wall gap. The wall-shear-stress distribution predicted numerically by the VELASCO code (Eifler & Nijsing (1974)) is also shown. This code models the momentum transport through the subchannel boundaries by anisotropic eddy viscosities and by an assumed single secondary-flow cell, although the anisotropic eddy-viscosity values are considerably smaller than the experimental data. The agreement between prediction and experimental results is poor for the gap between the rod and the wall ($\theta = 90°$, $x = 0$ mm). The numerical results greatly overpredict the minimum level of the wall shear stress for both the rod and the duct wall.

The effect of changing the wall gap width or $w/d$ ratio, while maintaining a fixed $p/d$ ratio of 1.071, is shown in figure 4(*a*) for the rod wall-shear-stress distribution. In the experimental data there is a systematic trend at $w/d$ ratios of 1.026, 1.048, 1.071, 1.096 and 1.118, the Reynolds numbers being 5.46, 7.57, 8.53, 10.7 and $10.5 \times 10^4$ respectively. The minimum stress in the rod-to-wall gap ($\theta = 90°$) changes relatively slowly for the three larger $w/d$ ratios, and there is a more marked reduction for $w/d$ ratios of 1.048 and 1.026. There is some evidence of a shift in the position

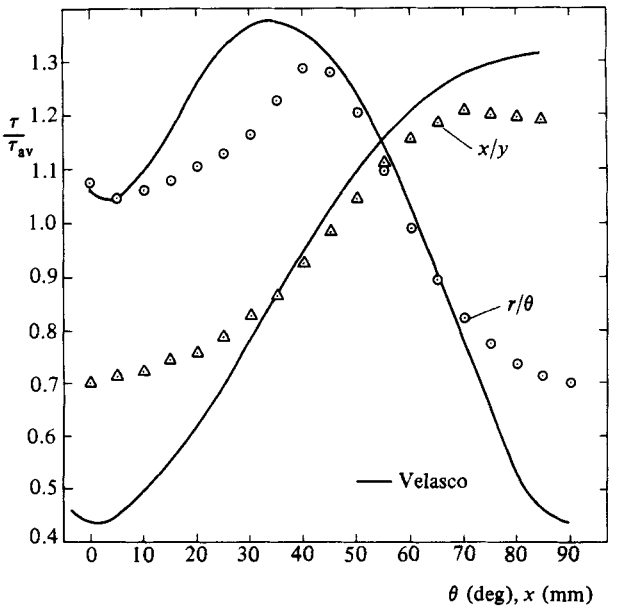


FIGURE 3. Wall-shear-stress variation; wall-bounded subchannel ($p/d = 1.071$; $w/d = 1.026$; $Re = 5.46 \times 10^4$).

of maximum rod wall shear towards the rod-to-wall gap region with decreasing $w/d$ ratio. The wall shear stress in the fixed geometry rod-to-rod gap region increases markedly as the $w/d$ ratio is reduced. This is due to the asymmetry of the interconnected subchannels for all $w/d$ ratios except 1.071, and the consequent momentum transport through the rod gap. The level of the duct wall shear stress (figure 4*b*) at the centre of the rod-to-wall gap, $x = 0$ mm, remains substantially independent of $w/d$ for $w/d$ ratios greater than 1.048.

### 3.2. *Reynolds stresses*

A significant finding of both experimental series was the systematic tendency for turbulence levels to increase in the corresponding rod-gap region as either the $p/d$ or $w/d$ ratio was reduced. This was shown by the selective amplification of three components of the Reynolds stresses. The signal-processing system employed by Rehme evaluated five of the Reynolds-stress components using the nonlinearized hot-wire anemometer output, and small-signal approximations to the probe response. Caution must be exercised in regions where the intensity reaches very high levels ($w/d = 1.026$ and $\theta > 50°$), as the approximations are then no longer accurate.

Following the convention accepted for incompressible flow, the r.m.s. level of the axial and azimuthal turbulent velocity components are normalized by the local wall friction velocity and the azimuthal Reynolds shear stress by the local wall shear stress. The distances $y$ from the wall are non-dimensionalized by the distance $\hat{y}$ between the wall and the experimentally determined line of maximum velocity. For reasons of space, only the Reynolds-stress components that show significant changes, the axial and azimuthal intensities and the azimuthal shear stress, are presented.

#### 3.2.1. *Axial turbulence intensity*

The axial turbulence-intensity distribution, for a Reynolds number of $7.60 \times 10^4$ and measured from the rod surface at a $p/d$ ratio of 1.036 and a $w/d$ ratio of 1.072

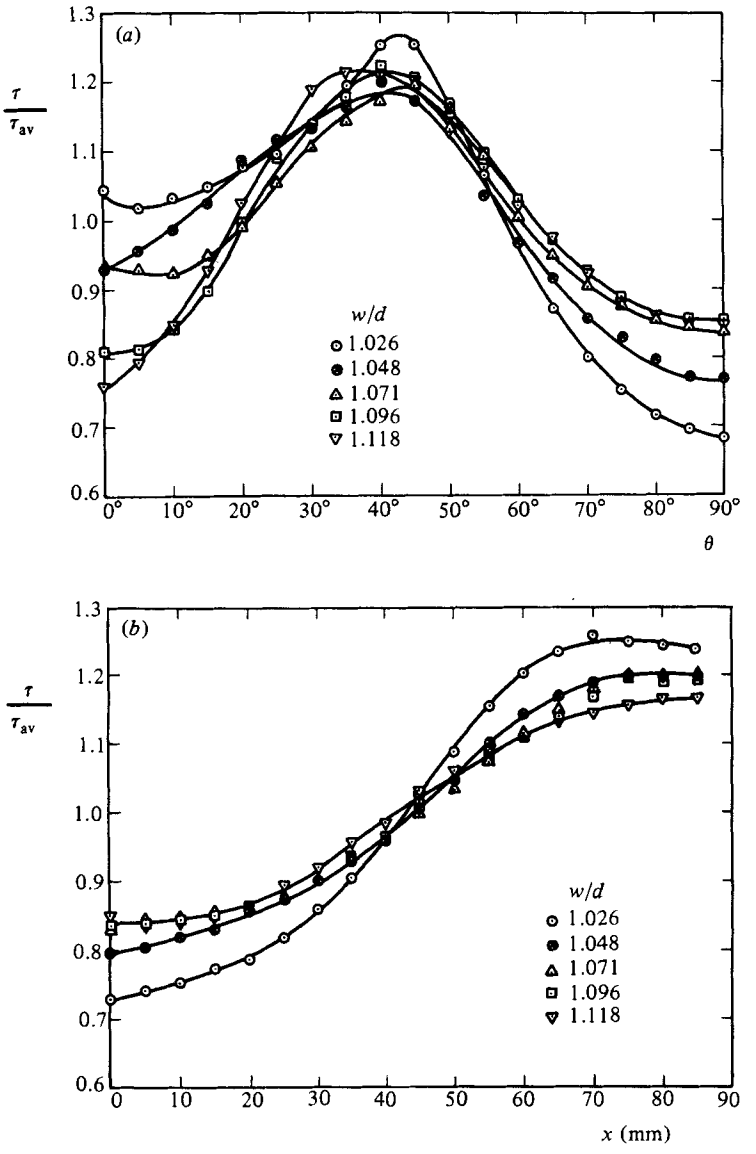


FIGURE 4. (*a*) Wall-shear-stress variation for the rod; wall-bounded subchannel ($p/d = 1.071$; $w/d = 1.026, 1.048, 1.071, 1.096, 1.118$; $Re = 5.46, 7.57, 8.53, 10.7, 10.5 \times 10^4$). (*b*) Wall-shear-stress variation for the duct wall; wall-bounded subchannel ($p/d = 1.071$; $w/d = 1.026, 1.048, 1.071, 1.096, 1.118$; $Re = 5.46, 7.57, 8.53, 10.7, 10.5 \times 10^4$).

(Rehme 1982*c*), is shown in figure 5(*a*). The axial turbulence intensity reaches high levels, and, for the rod-to-rod gap region, the traverses at 15° and 20° increases with increasing wall distance, implying a source that is not associated with the normal wall generation mechanism. The maximum level of axial intensity, scaled by the local wall shear stress, is also located in the centre of the gap for traverses between 15° and 20°. For the wider rod-to-wall gap, the distribution is higher than that established by Lawn (1971) for developed turbulent pipe flow.

The axial turbulence-intensity distribution for the narrowest rod-to-wall gap ($w/d = 1.026, p/d = 1.071$; Rehme 1982*b*) is shown in figure 5(*b*). The intensity in the

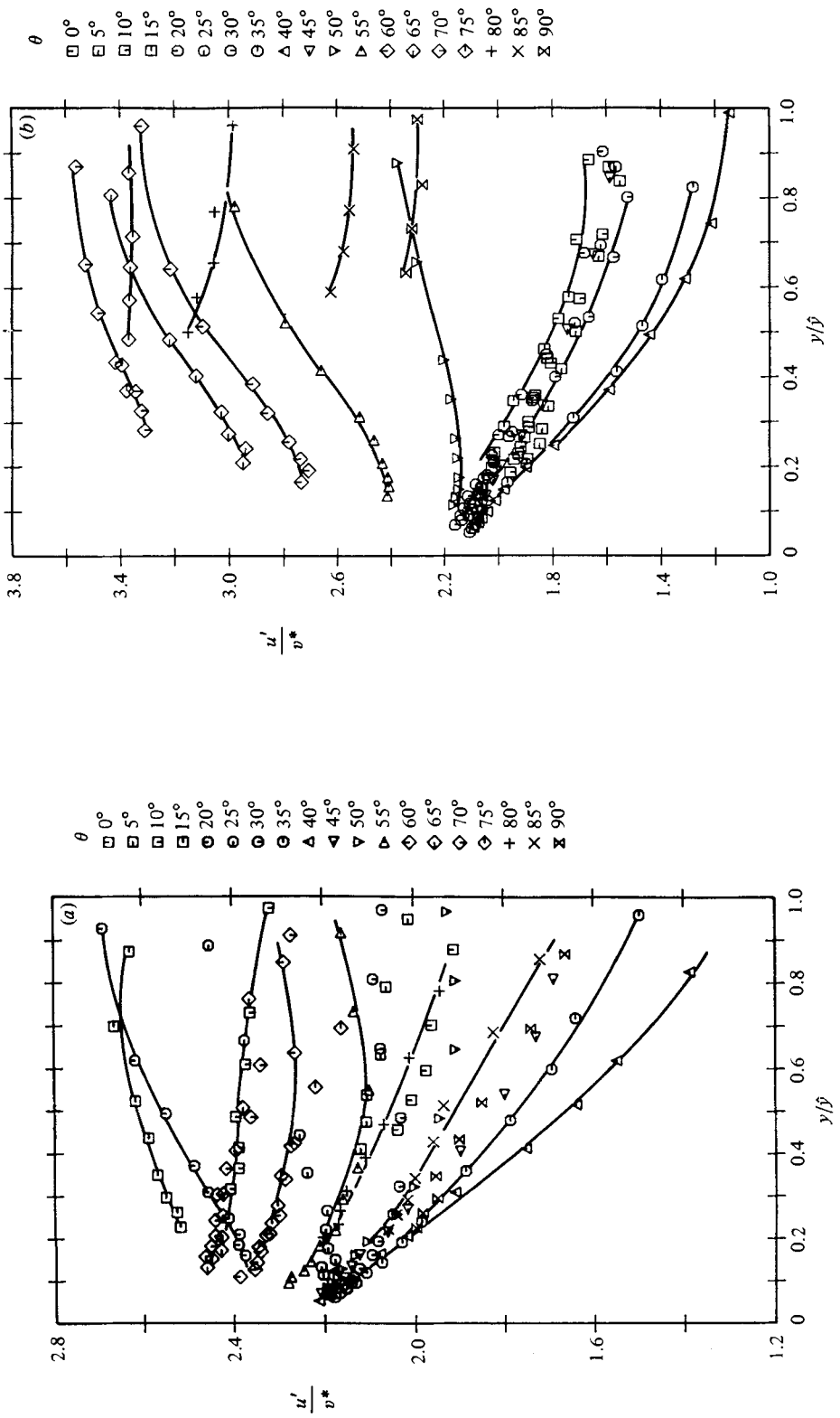


FIGURE 5. (*a*) Axial turbulence-intensity distribution; wall-bounded subchannel, rod-centred cylindrical coordinate system ($p/d = 1.036$; $w/d = 1.072$; $Re = 7.60 \times 10^4$). (*b*) Axial turbulence-intensity distribution; wall-bounded subchannel, rod-centred cylindrical coordinate system ($w/d = 1.026$; $p/d = 1.071$; $Re = 5.46 \times 10^4$).

rod-to-wall gap reaches extremely high levels, with a local maxima for the traverse at 70°. For traverses between 50° and 70°, the axial intensity increases with increasing wall distance, again suggesting a generating mechanism that is not directly coupled to the local rod wall. The intensity distribution in the relatively open rod-to-rod gap is also higher than the corresponding pipe-flow data of Lawn (1971).

The variation of the axial turbulence intensity along the maximum velocity line for a fixed $p/d$ ratio of 1.071 and $w/d$ ratios between 1.026 and 1.118 is shown in figure 6. The following two trends are evident.

(i) In the region between the rods (0°–35°), the axial intensity increases with increasing $w/d$, although the geometry remains unchanged in this region.

(ii) In the area between the rod and channel walls (40°–90°), the axial intensity increases strongly with decreasing $w/d$ ratio. The absolute values for $w/d = 1.026$ should be treated with caution owing to the high intensity levels.

A further feature is the almost fixed location of the point of the minimum axial turbulence intensity between 35° and 40°, for the maximum-velocity line.

### 3.2.2. *Azimuthal turbulence intensity*

The distribution of the azimuthal turbulence intensity for the maximum velocity line, and for a fixed $p/d$ ratio of 1.071 with $w/d$ ratios in the range 1.026–1.118, is shown in figure 7.

The dominant feature of the results is that the azimuthal intensity for the rod-to-wall gap region increases as the $w/d$ ratio decreases. The peak of the azimuthal intensity is located in the centre of the rod-to-wall gap (90°) and, for $w/d$ ratios of 1.071 or less at this location, is apparently of greater magnitude than the axial turbulence intensity. The very high azimuthal intensities in the rod-to-wall gap for the low $w/d$ ratio studies indicate that the quantitative levels are inaccurate owing to the failure of the small-signal approximations. It is probable that a structural feature of the flow, acting in the narrow gap, is selectively amplifying the $-\rho\overline{w^2}$ component of the Reynolds stresses.

The local minima in the azimuthal intensity for the maximum velocity line is between 35° and 40°, coincident with the location of the minimum axial intensity. In the fixed geometry rod-to-rod gap the azimuthal intensity distribution is relatively independent of the $w/d$ ratio.

### 3.2.3. *Azimuthal Reynolds shear stress*

The distribution of the azimuthal component of the Reynolds shear stresses for rod-centred polar coordinates in a symmetrical test section ($p/d = 1.036$, $w/d = 1.072$; Rehme 1982*c*) is shown in figure 8 for a Reynolds number of $7.60 \times 10^4$. Symmetry requires $-\rho\overline{uw}$ to be zero for the radial traverse at 0°, the centre of the rod-to-rod gap area; this condition was not satisfied experimentally. A most remarkable feature of the data, however, is the very high azimuthal gradient of $-\rho\overline{uw}$ for radial traverses between 0° and 10°. In view of this gradient, and because of the relatively small level of $-\rho\overline{uw}$ for the 0° traverse compared with the extreme levels reached in the immediately adjacent region of the rod-to-rod gap, the lack of symmetry is unimportant. The peak value of the azimuthal Reynolds shear stress is for the centre of the traverse at 15°, where it is approximately a factor of 3.2 greater than the local wall shear stress. Because of the inaccuracy of anemometer small-signal approximations for the axial and azimuthal turbulence intensities reached in this area, the absolute levels of $-\rho\overline{uw}$ should again be viewed with caution. There is strong evidence, however, of a powerful and energetic structure in the fluid for both narrow rod-to-rod and rod-to-wall gap areas.

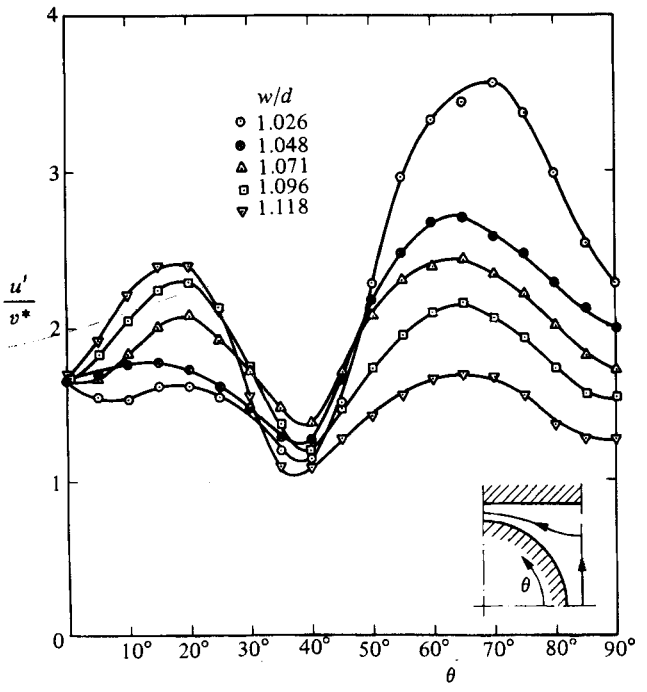


FIGURE 6. Axial turbulence-intensity distribution in the wall-bounded subchannel for the maximum-velocity line ($p/d = 1.071$; $w/d = 1.026$, 1.048, 1.071, 1.096, 1.118; $Re = 5.46$, 7.57, 8.53, 10.7, $10.5 \times 10^4$).

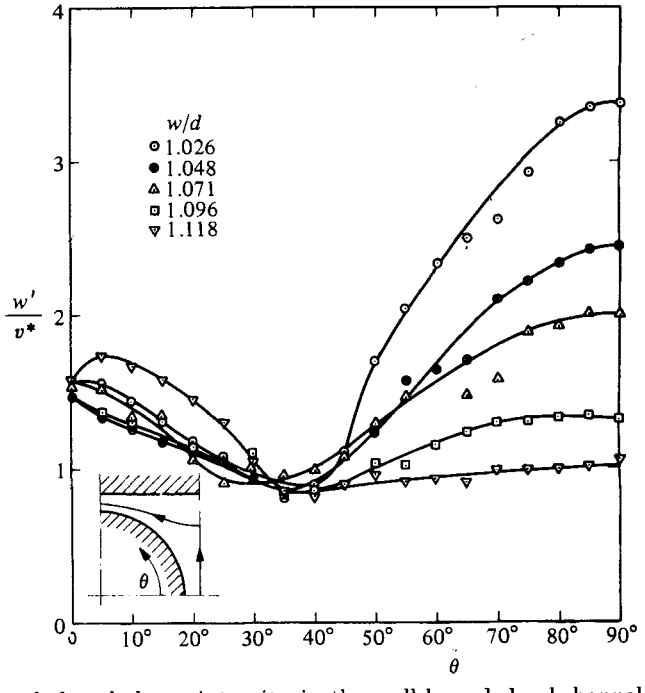


FIGURE 7. Azimuthal turbulence intensity in the wall-bounded subchannel distribution for the maximum-velocity line ($p/d = 1.071$; $w/d = 1.026$, 1.048, 1.071, 1.096, 1.118; $Re = 5.46$, 7.57, 8.53, 10.7, $10.5 \times 10^4$).

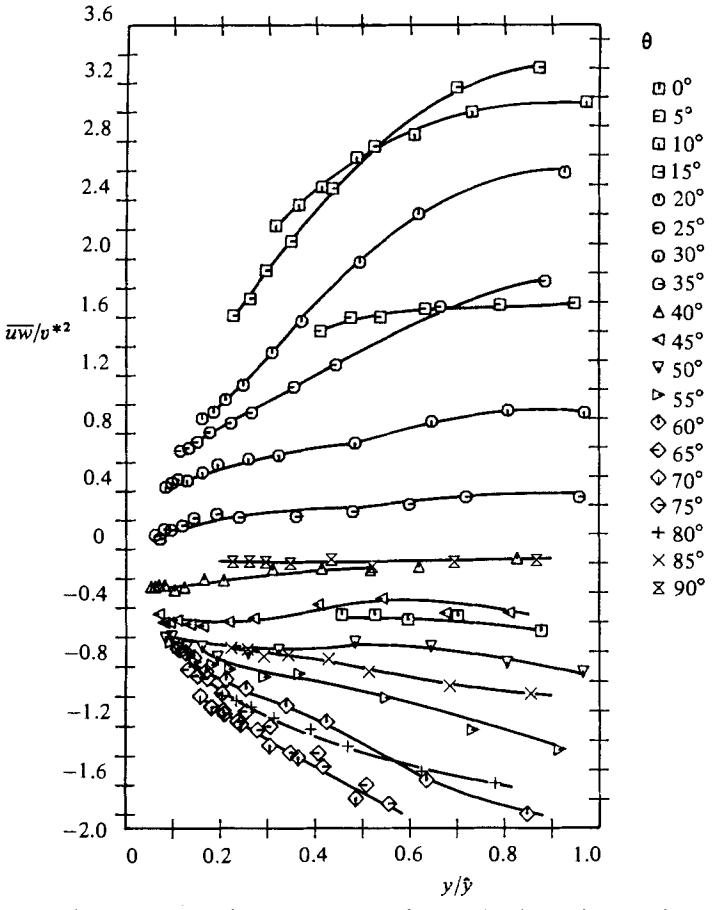


FIGURE 8. Azimuthal Reynolds shear-stress distribution in the wall-bounded subchannel ($p/d = 1.036$; $w/d = 1.072$; $Re = 7.60 \times 10^4$).

It is necessary to question whether this flow feature can be linked to, or shown to be a result of, mean secondary-flow cells directing higher-momentum fluid from the subchannel centre to the rod-to-rod gap area. The technique used to position the slant wire probe accurately, and the instrumentation used to measure the mean anemometer bridge voltage at the quadrature positions, were substantially the same as those adopted by Seale (1982). Despite the precision of the measurement system, there was little evidence of significant secondary-flow velocities in the rod-to-rod gap region. If mean secondary-flow cells are to be associated with the increasingly high turbulence-intensity levels caused in the rod gap by reduction of the $w/d$ ratio or $p/d$ ratio, there should be a corresponding trend towards a higher magnitude of the mean secondary-flow components. No such trend was evident.

## 4. Experimental results; square-pitch rod cluster

Experimental data are given for the open rod gap of the symmetrical square-pitch rod cluster, $p/d = 1.107$. These results are from an extensive investigation of the flow structure in the open rod-gap area at four Reynolds numbers in the range $22.6 \times 10^3$–$207.6 \times 10^3$ (Hooper, Wood & Crawford 1983).

The Reynolds-stress distribution for the open rod gap had the same general features

as the wall-bounded rod array; however, for all traverses the turbulence intensity levels were sufficiently small to allow accurate use of the hot-wire anemometer small-signal approximations. This was demonstrated by taking either one or five redundant hot-wire measurements for each duct position (Hooper 1980*a*) and showing the self-consistency of the Reynolds-stress measurements.

### 4.1. *Axial turbulence intensity*

The axial turbulence intensity, for a Reynolds number of $133 \times 10^3$ and the central region of the open rod gap between $-15°$ and $15°$, is given in figure 9. There is some evidence of asymmetry in the axial turbulence-intensity distribution about the symmetry axis (and subchannel boundary) at 0°, with levels being slightly higher for positive than for negative traverse angles. These features are present in each of the four Reynolds numbers (Hooper *et al.* 1983), and may be associated with some asymmetry of the large-scale structure of the axial component in the rod gap (Wood & Hooper 1984).

The local maxima for the axial turbulence intensity is for traverses at $\pm 15°$, and the minima is at 0°. Consistent with results from the Rehme experimental series, the axial turbulence-intensity values are considerably higher than the pipe-flow results of Lawn (1971) and Laufer (1954) for the whole area of the rod gap remote from the rod wall. The axial intensity seems to approach the pipe-flow distribution in the vicinity of the rod wall. This distribution suggests the possible superposition of two generation processes for $-\rho\overline{u^2}$. The normal turbulence-generation mechanism is present in the high mean-axial-velocity gradient near the rod wall, but another process is active in the central region of the gap.

### 4.2. *Azimuthal turbulence intensity*

The azimuthal turbulence-intensity distribution for a Reynolds number of $133 \times 10^3$ is reasonably symmetric about the 0° traverse (figure 10). The distribution for traverses at $\pm 15°$ is below the local maxima at 0°, and is the reverse of the trend of the axial turbulence intensity results. The $-15°$ traverse results are generally larger than the corresponding positive angle traverse. The results for the four Reynolds numbers show these features, although the separation between the 0° and $\pm 15°$ traverse data is somewhat marginal. The azimuthal intensity is considerably higher than the pipe-flow results of Lawn (1971) and Laufer (1954) and essentially independent of the wall distance.

### 4.3. *Azimuthal Reynolds shear stress*

The azimuthal Reynolds shear stress (figure 11) shows good antisymmetry about the 0° traverse, and is almost zero at the subchannel boundary. The remarkable increase in the magnitude of the $-\rho\overline{uw}$ Reynolds-stress component away from the symmetry axis, to a maximum of $\pm 1.5\tau_w$ for the $\pm 15°$ traverses, is also shown. This feature is common to the four Reynolds numbers (Hooper *et al.* 1983), and is perhaps the most interesting feature of the Reynolds-stress distribution.

In this test section, to an accuracy of $\pm 1\%$ of the local axial velocity (Hooper 1980*a*,*b*; Hooper *et al.* 1983), no non-zero secondary-flow components were resolved. The open rod-to-rod gap results of Seale (1982) showed secondary-flow velocities considerably below this limit. However, using an integral form of the axial momentum equation developed by Wood & Hooper (1984), the very high contribution of the azimuthal gradient of $-\rho\overline{uw}$ to the axial momentum balance was shown for the 0° traverse.

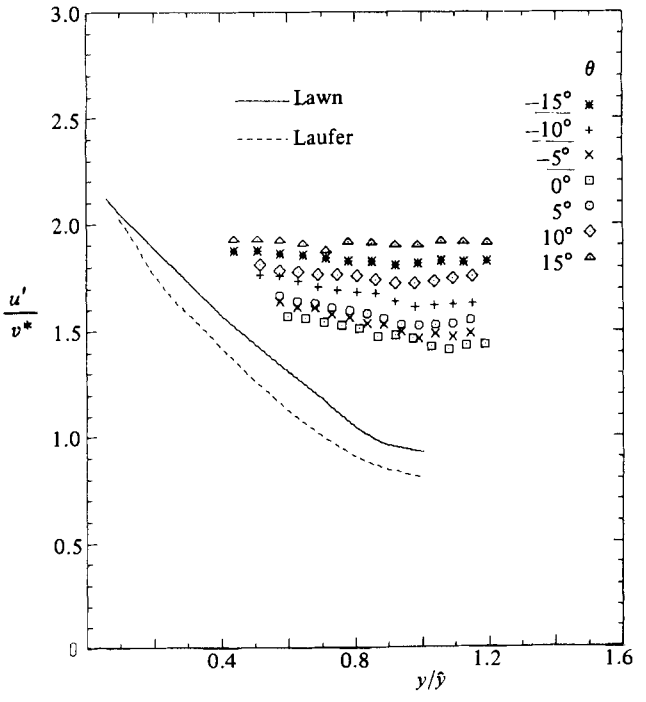


FIGURE 9. Axial turbulence-intensity distribution; symmetrical square-pitch rod array ($p/d = 1.107$; $Re = 13.3 \times 10^4$).

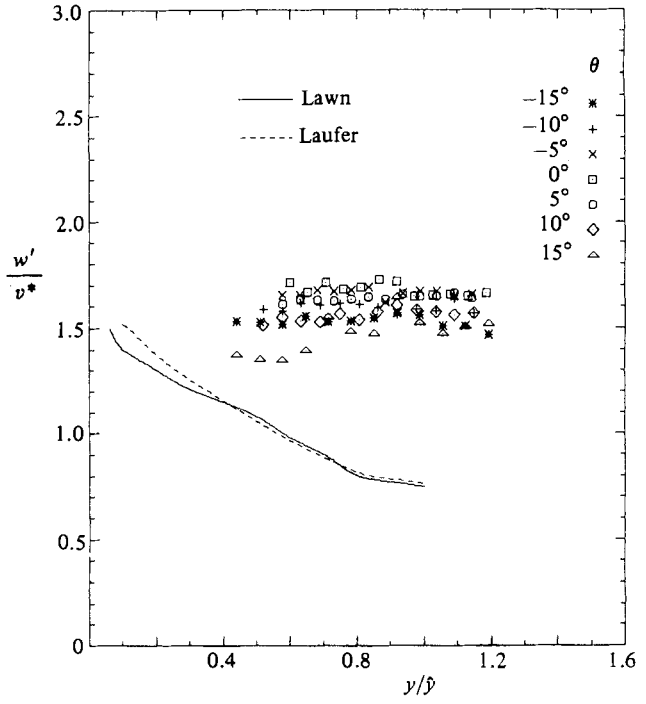


FIGURE 10. Azimuthal turbulence-intensity distribution; symmetrical square-pitch rod array ($p/d = 1.107$; $Re = 13.3 \times 10^4$).

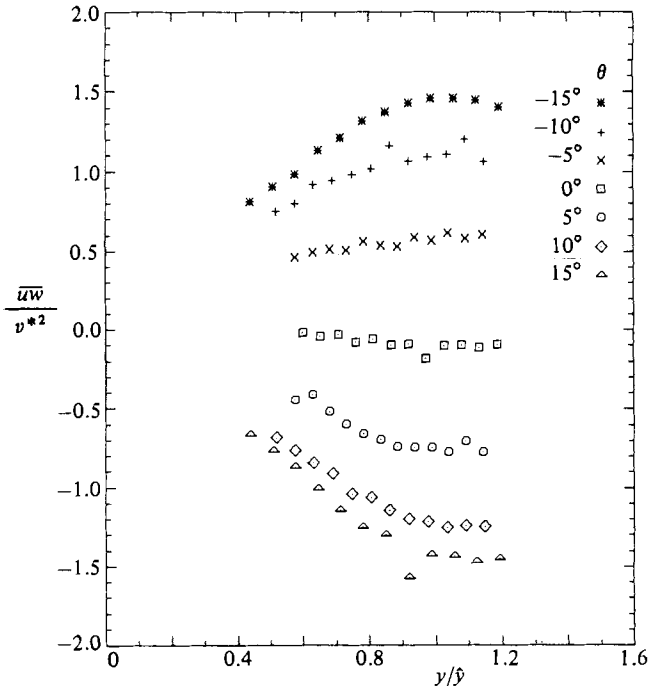


FIGURE 11. Azimuthal Reynolds shear-stress distribution; symmetrical square-pitch rod array ($p/d = 1.107$; $Re = 13.3 \times 10^4$).

### 4.4. *Axial-vorticity source term*

The source term for an axial vorticity component, resolved in a rod-centred cylindrical polar coordinate system, is

$$\frac{\rho}{r}\frac{\partial}{\partial\theta}\frac{1}{r}\frac{\partial}{\partial r}r(\overline{v^2}-\overline{w^2})+\frac{\rho}{r}\frac{\partial}{\partial\theta}\frac{1}{r}\frac{\partial}{\partial\theta}(\overline{vw})-\frac{\rho}{r}\frac{\partial}{\partial r}r\frac{\partial}{\partial r}(\overline{vw})-\frac{2\rho}{r}\frac{\partial}{\partial r}(\overline{vw}). \tag{1}$$

Previous studies, summarized by Haque *et al.* (1983) suggest principally that the difference of the normal Reynolds stresses $-\rho(\overline{w^2}-\overline{v^2})$ is the production term of (1). The equations for these normal Reynolds-stress components contain possible source terms involving the radial or azimuthal gradient of the mean axial velocity (Wood & Hooper 1984), whereas this is not the case with the planar Reynolds shear stress $-\rho\overline{vw}$. Although the potential source term for $-\rho\overline{vw}$ is comparatively small, experimental data from the symmetrical square-pitch array ($p/d = 1.107$) showed non-zero levels of $-\rho\overline{vw}$ in the open rod gap for each of the four Reynolds numbers (Hooper 1980*a*, *b*; Hooper *et al.* 1983). Approximate antisymmetry was shown by the $-\rho\overline{vw}$ results with respect to the symmetry boundary at 0°, but the accuracy was poor. The planar Reynolds shear stress became effectively zero for traverse angles with $|\theta| > 25°$.

The argument of Haque *et al.* (1983), referred to in §1, cannot be extrapolated to the closely spaced rod-array geometry since, as the $p/d$ ratio is reduced, the distribution of the $-\rho(\overline{w^2}-\overline{v^2})$ term of (1) becomes increasingly different from the radial axisymmetric pipe-flow results. This difference consists primarily of the amplification of the azimuthal component of the normal Reynolds stresses $-\rho\overline{w^2}$ to extremely high levels in the centre of the rod gap, with no corresponding increase

in the radial component $-\rho\overline{v^2}$. Indeed, the results of the wall-bounded subchannel array show that $-\rho\overline{v^2}$ decreases in magnitude for low $p/d$ ratios in the open rod-to-rod gap, although this may simply be linked to the failure of the small-signal approximations. The increasingly high level of the wall-shear-stress variation, coupled with the greater difference in $-\rho(\overline{w^2}-\overline{v^2})$, suggests, however, that the source term for an axial vorticity component is highest in the open rod-to-rod gap area.

The results for the square pitch array at a Reynolds number of $22.6\times10^3$ ($p/d = 1.107$) are shown in figure 12($a$,$b$), in which $-\rho(\overline{w^2}-\overline{v^2})$ is normalized by the average and not the local wall shear stress. The partial derivative of the azimuthal gradient appears to reach the highest levels at the centre of the open rod-to-rod gap. Non-zero secondary flow was not measured directly in this region by the inclined hot-wire anemometry to $\pm1$ % of the local axial mean velocity. Consideration of the axial-momentum balance (Hooper 1980$a$; Wood 1981; Wood & Hooper 1984) showed that the $V$-component for the 0° traverse is below the maximum of 0.5 % of the local axial velocity as, by symmetry, the azimuthal component of secondary flow $W$ must be zero for this traverse.

A further experimental method was developed by Hooper (1980$a$) in an attempt to resolve $W$ directly. The dispersion and possible azimuthal translation of a nitrous oxide gas plume injected parallel to the rod axis and near the surface of the central rod in the symmetrical square pitch rod array was measured by an infrared gas analyser. This technique is capable of resolving an azimuthal secondary-flow velocity $W$ of $\pm0.5$ % of the local axial velocity component $U$. Gas injection was made for $\theta$ equal to 0 and $+15°$, with no azimuthal translation resolved for either injection angle. The plume was measured 0.5 m downstream from the injection point, and the data were fitted by a least-squares numerical routine to a Gaussian shape. The result at 0° confirms the symmetry of the test section; Hooper (1980$a$) initially considered that the result at 15° indicated multiple secondary flow cells in the open rod-to-rod gap area. The mean azimuthal eddy mass diffusivity, calculated from the plume shape, was the same magnitude, within experimental error, for the two injection angles.

The mass-diffusion results for the rod gap indicated that the turbulent-diffusion rates in the azimuthal direction are approximately independent of azimuthal angle, for locations equidistant from the rod surface. This feature may be explained by the presence of multiple secondary flow cells, although the wall-bounded subchannel results showed that no consistent nor even measurable secondary flow cells in the rod gap were associated with the very high turbulence levels reached at low $p/d$ or $w/d$ ratios.

## 5. Structural analysis of the turbulent-velocity components

The flow mechanism responsible for the generation of increasingly high turbulence intensities in the open rod gap, as the rod spacing or wall distance ($p/d$ or $w/d$ ratio) is reduced, can be better understood through a structural analysis of the turbulent flow. The analysis was made for both test sections in a Cartesian coordinate system, with the origin located at the centre of the rod-to-rod gap. The $x$-axis was coincident with the radial traverse at 0°, and the $z$-axis remained the duct axis.

### 5.1. *Wall-bounded rod array*

A symmetrical test-section geometry, with equal rod-to-wall distances ($w/d$ ratio of 1.072) was used for the structural analysis of the wall-bounded rod array. The $p/d$ ratio was 1.036, and the Reynolds number was $7.6\times10^4$; these values are equivalent

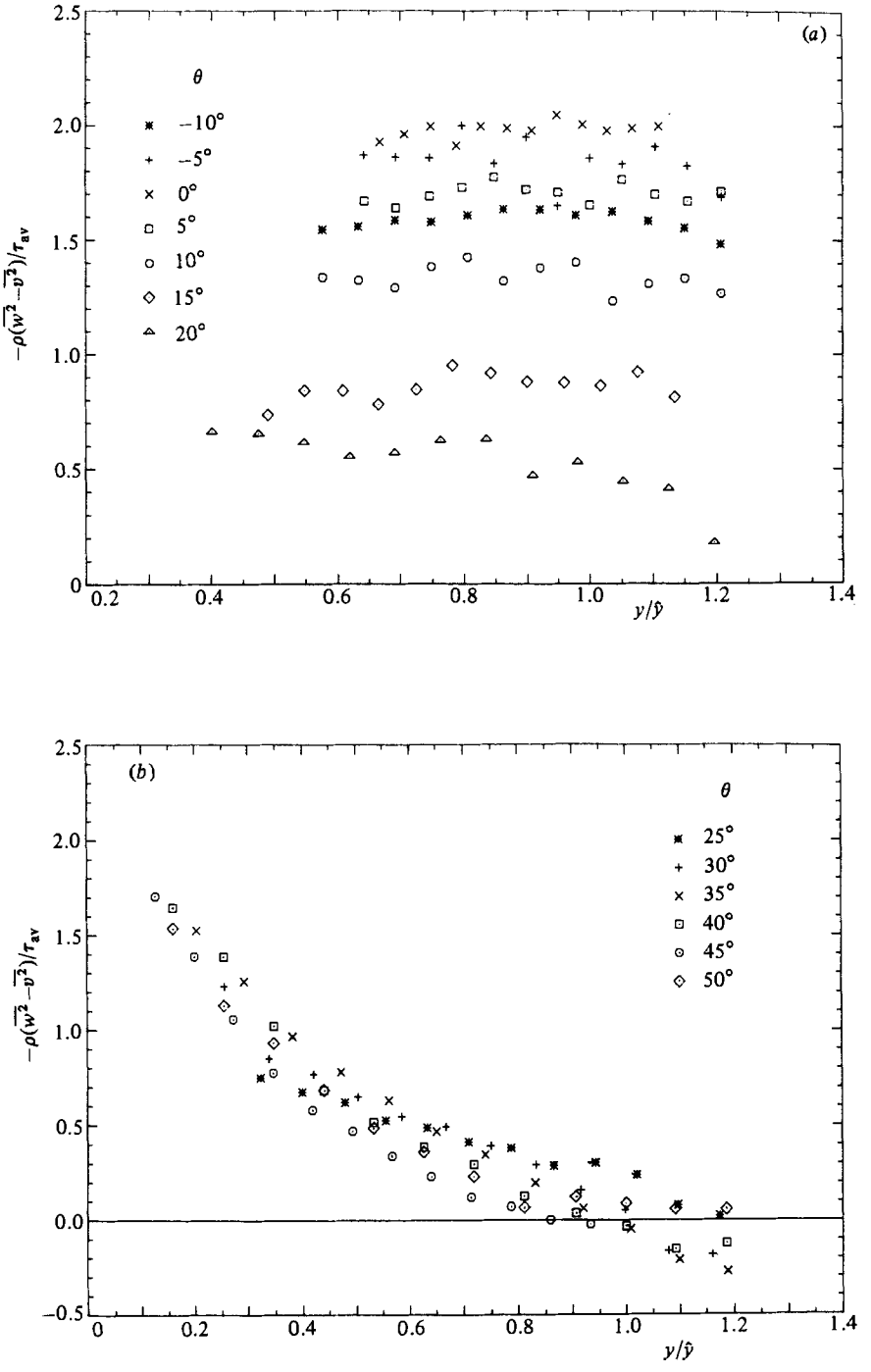


FIGURE 12. (*a*) Axial-vorticity source term $-\rho(\overline{w^2}-\overline{v^2})$, normalized by average rod wall shear stress; symmetrical square-pitch rod array ($p/d = 1.107$; $Re = 2.26 \times 10^4$). (*b*) Axial-vorticity source term $-\rho(\overline{w^2}-\overline{v^2})$, normalized by average rod wall shear stress; symmetrical square-pitch rod ($p/d = 1.107$, $Re = 2.26 \times 10^4$).

to those used by Rehme (1982*c*), who gives details of the mean-flow structure and the distribution of five of the Reynolds-stress components.

Two hot-wire probes were used to establish the auto- and cross-correlation functions. Each probe had a single normal wire and a single slant-wire element. Details of the probe-manufacturing and -calibration technique and the small-signal approximations are given by Hooper (1980*a*). It is noted that the high turbulence intensity levels in the rod-to-rod gap limit the accuracy of these approximations, so, for this geometry, the experimental results must be regarded as qualitative.

5.1.1. *Direct reproduction of turbulent-velocity components*

The turbulent-velocity components recorded simultaneously at two positions in the rod gap, point 2 located at $(x, y)$-coordinates of $(0, -10\text{ mm})$ and point 4 at $(0, 10\text{ mm})$, are shown in figures 13 (*a*,*b*). The signals were recorded on an EMI 7000 series FM tape recorder, and, after allowing for the 64:1 tape speed down ratio, the plotting system was able to display components to approximately 2 kHz.

Figure 13 (*a*) clearly shows that the axial turbulent velocity component $u$ has a large-scale structure for both locations in the $(x, z)$-plane. The mean axial velocity at these locations is $20.5\text{ m s}^{-1}$, and the peak excursion of the axial turbulence component $u$ is approximately 25 % of this value.

The turbulence component $v$ along the $x$-axis is considerably reduced in magnitude, and there is little evidence of the large-scale structure that the axial component has. The $v$-component is more typical of the non-axial turbulent velocity components for developed internal duct flow at high Reynolds numbers. The lack of a large-scale structure and reduced intensity for $v$ in the rod gap is not surprising; this component is directed essentially towards the rod wall, and the narrow gap must dampen and restrict velocity fluctuations normal to the rod surface.

The turbulent-velocity component $w$, directed through the rod gap along the $y$-axis, is seen in figure 13 (*b*) to have an almost-periodic large-scale structure. The magnitude of the velocity fluctuations in $w$ is at least equal to that of the axial-velocity fluctuation at both locations. There is apparently more fine-scale turbulence superimposed on the transverse or $w$-component than on $u$. Clearly, the large-scale structure of $w$ is highly correlated across the duct symmetry or $x$-axis. The presence of an energetic, large-scale and almost periodic momentum exchange process through the rod-to-rod gap is strongly suggested by the large-scale structure of $w$.

5.1.2. *Cross-correlation study within one subchannel*

To resolve the extent of penetration of the large-scale structure in the rod gap into the subchannel, the cross-correlation coefficients between the same velocity components were measured along the $y$-axis within one subchannel. A fixed hot-wire probe was located at $(x, y)$-coordinates of $(0, 10\text{ mm})$ and a second probe traversed the $y$-axis to $(0, 55\text{ mm})$. An analogue signal-processing technique was used to generate the normalized cross-correlation coefficients, so that all the higher-frequency components of the turbulence, which are unlikely to correlate over large distances, contributed to individual signal variances.

The axial turbulent-velocity component $u$ is significantly correlated for a considerable distance from the rod gap (figure 14). The furthest data point corresponds to the intersection of a radial traverse at 35° and the subchannel maximum velocity line. The results of Rehme (1982*c*) showed a significant reduction in the axial intensity for this region.

The transverse turbulent-velocity component $w$, directed through the rod gap, is

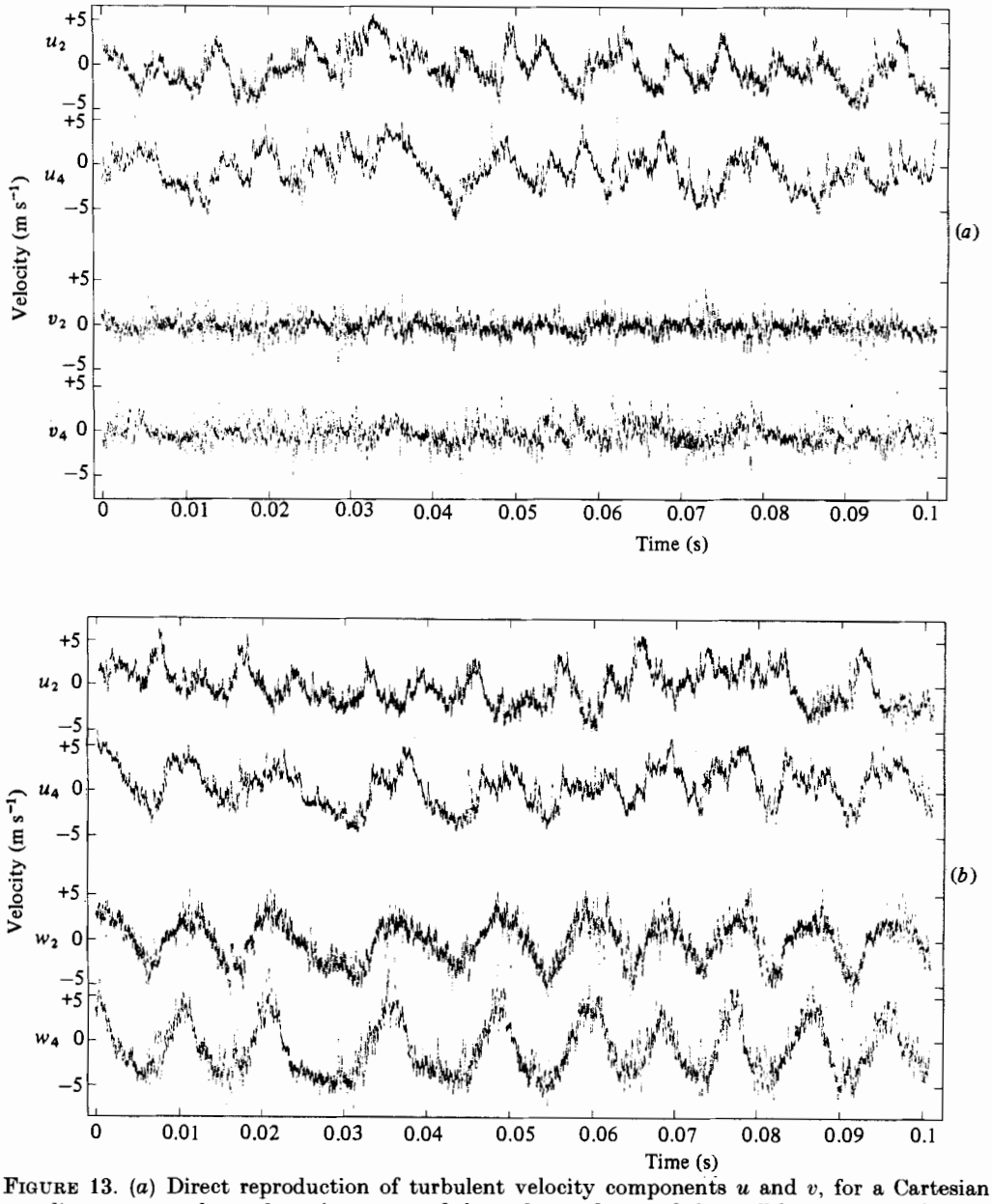


FIGURE 13. (*a*) Direct reproduction of turbulent velocity components $u$ and $v$, for a Cartesian coordinate system located at the centre of the rod-to-rod gap of the wall-bounded subchannel ($p/d = 1.036$; $w/d = 1.072$; $Re = 7.60 \times 10^4$). (*b*) Direct reproduction of turbulent-velocity components $u$ and $w$, for a Cartesian coordinate system located at the centre of the rod-to-rod gap of the wall-bounded subchannel ($p/d = 1.036$; $w/d = 1.072$; $Re = 7.60 \times 10^4$).

also well correlated over the same distance. The cyclic intersubchannel momentum-exchange process apparently extends over a considerable region of the subchannel. In view of the lengthscales of $u$ and $w$, the turbulent structures in the rod-to-rod and rod-to-wall gap regions may be coupled.

The $x$-axis or $v$-component of turbulence has no significant spatial cross-correlation, which is to be expected since $v$ has no large-scale structure.

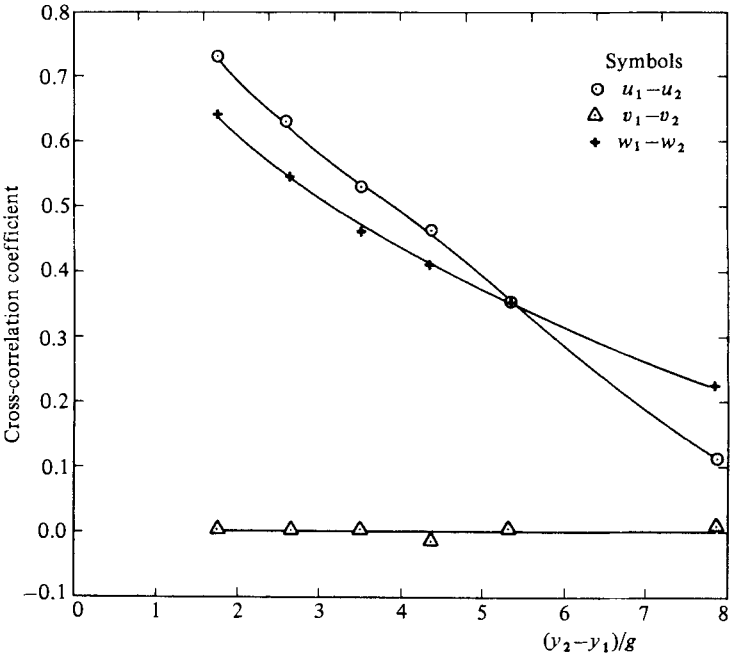


FIGURE 14. Spatial correlation of $u$, $v$ and $w$ for the rod-gap region, wall-bounded subchannel ($p/d = 1.036$; $w/d = 1.072$; $Re = 7.60 \times 10^4$).

### 5.1.3. *Autocorrelation functions*

The autocorrelation functions of the axial and transverse velocity components ($u$ and $w$) were computed at four positions on the $y$-axis, labelled $1, \ldots, 4$ and corresponding to $y$-distances of 0, $-10$, 5 and 10 mm. One hot-wire probe was fixed at location 2, and the other probe traversed the other positions. Positions 3 and 4 corresponded to rod-centred cylindrical coordinate traverse angles of 3.5° and 7° respectively; consequently there was little rotation of the axes between the two coordinate systems. The digital analysis system had a digitization rate of 2048 Hz, anti-aliasing prefilters set at 736 Hz and a record length of 100 seconds.

The autocorrelation functions for the axial turbulent-velocity component $u$ are shown in figures 15(*a–d*). For location 1 the $x$-axis or subchannel boundary, there is little evidence of a periodic structure to $u$. For locations 2 and 4 the axial turbulence autocorrelation function indicates a periodic component with a frequency of 92 Hz. This frequency is repeated in all the periodic auto- and cross-correlation functions measured, and represents an average frequency of the cyclic subchannel momentum exchange process for the particular Reynolds number. Rowe (1973) noted a similar periodic component in the autocorrelation functions for the axial turbulence-velocity component. This was present in the rod-gap region of the square-pitch array, but only for the lower $p/d$ ratio of 1.125.

The transverse turbulent velocity $w$ has a periodic autocorrelation at the four locations (figures 16(*a–d*), with strong evidence of the 92 Hz frequency component.

### 5.1.4. *Spatial cross-correlation functions*

The spatial cross-correlation between the axial turbulent-velocity fluctuations at locations 1 and 2 (figure 17*a*) indicates a relatively high correlation with little evidence of the dominant periodic component. For locations 2 and 4, which are

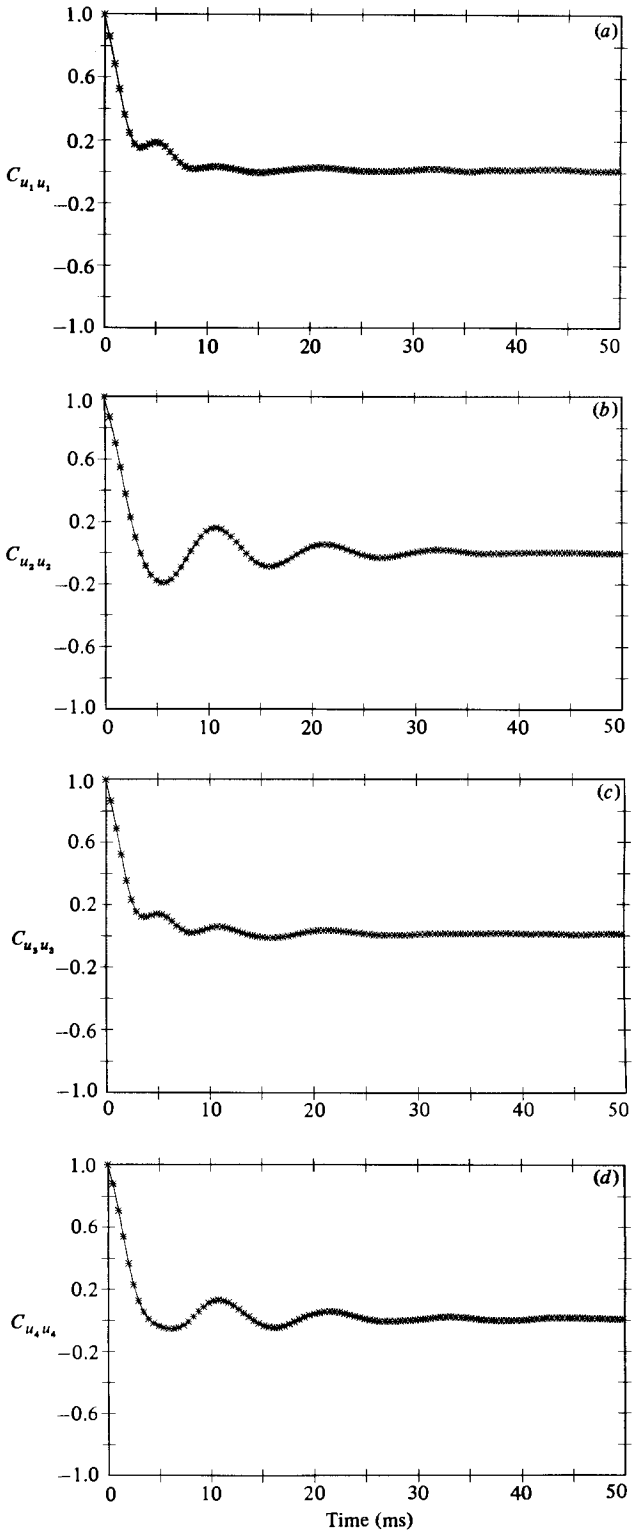


FIGURE 15. Axial turbulent-velocity $u$-autocorrelation; wall-bounded subchannel: (*a*) location 1; (*b*) location 2; (*c*) location 3; (*d*) location 4.

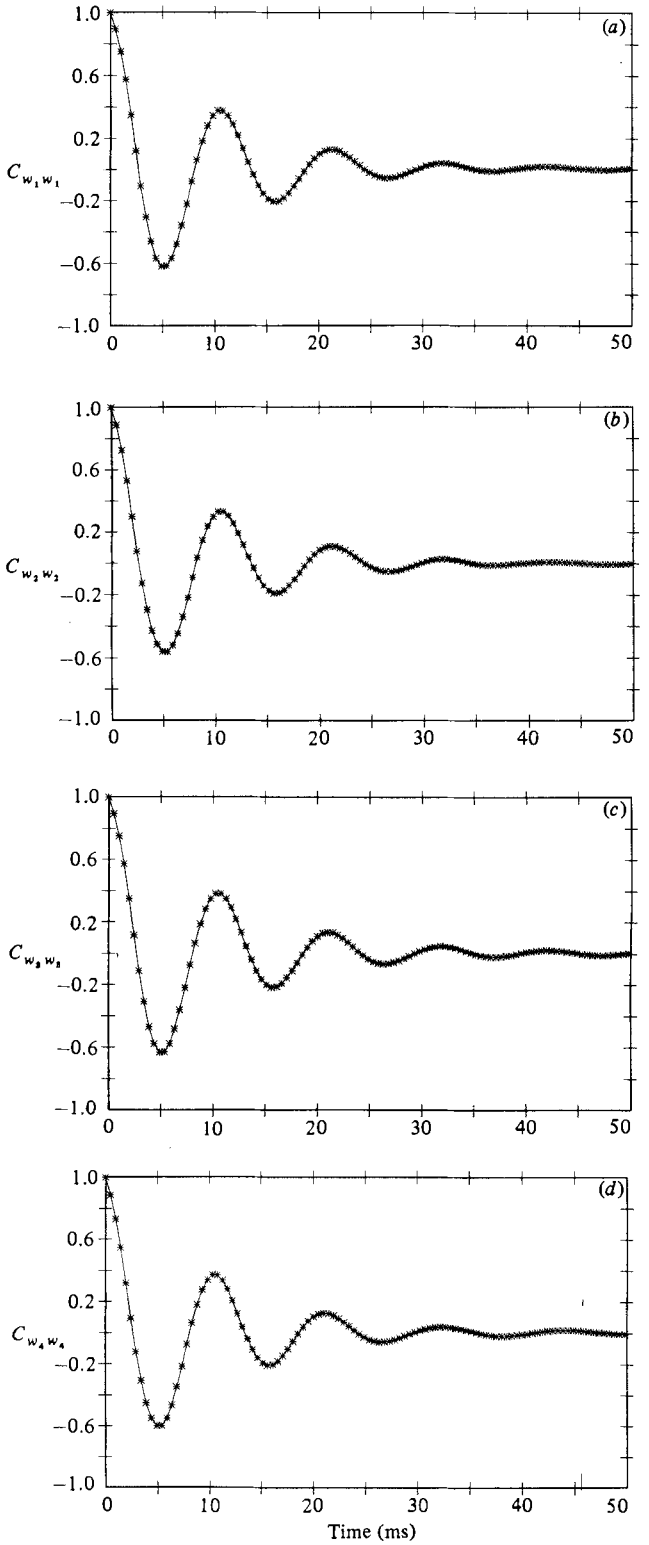


FIGURE 16. Transverse turbulent-velocity $w$-autocorrelation; wall-bounded subchannel: (*a*) location 1; (*b*) location 2; (*c*) location 3; (*d*) location 4.

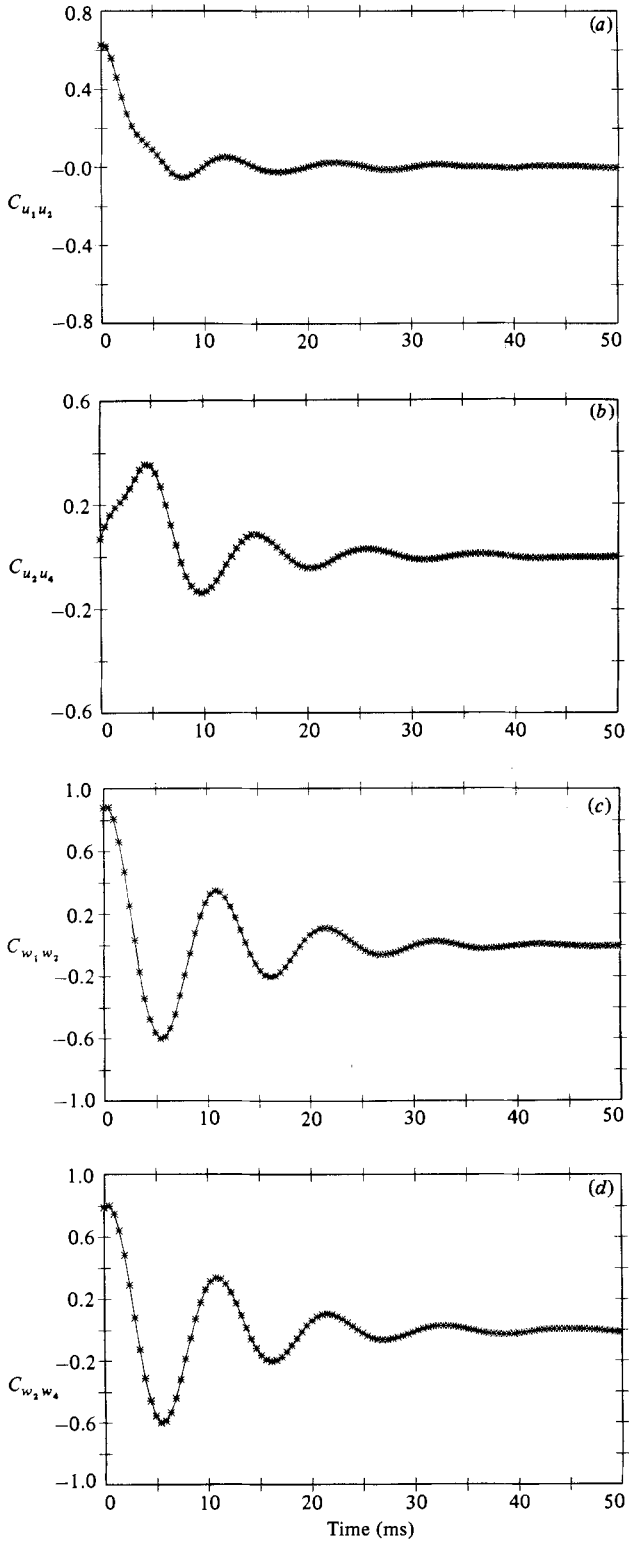


FIGURE 17. Spatial cross-correlation function; wall-bounded subchannel: (*a*) $u_1u_2$, locations 1 and 2; (*b*) $u_2u_4$, locations 2 and 4; (*c*) $w_1w_2$, locations 1 and 2; (*d*) $w_2w_4$, locations 2 and 4.

equidistant from the $x$-axis, the cross-correlation function (figure 17$b$) provides evidence of the periodic component, although at a reduced magnitude. A phase shift of approximately 45° between these locations for the periodic component of $u$ is also shown.

The transverse turbulent velocity cross-correlation function for both locations (figures 17$c,d$) strongly indicates the high spatial correlation of the periodic component through the rod gap, but there is little evidence of a phase difference in $w$ between locations 2 and 4 (figure 17$d$). There is also very little attenuation of the large-scale structure of $w$ over a lengthscale that is 3.5 times the rod-gap width.

#### 5.1.5. *Azimuthal Reynolds shear stress*

As was demonstrated experimentally, the azimuthal Reynolds shear-stress component $-\rho\overline{uw}$, in a rod-centred cylindrical coordinate system, is antisymmetric with reference to the 0° traverse or subchannel boundary. The axial rotation between this coordinate system at locations 2 and 4 and the gap-centred Cartesian system is only $\pm 7°$, with no rotation for position 1. The cross-correlation functions between $u$ and $w$ in the Cartesian system (figures 18$b,c$) show that this antisymmetry is associated with an 180° phase shift between $u$ and $w$ for locations 2 and 4. For location 1 on the $x$-axis or symmetry boundary, the phase shift is 90°, giving a value of zero when there is no time delay in the cross-correlation function (figure 18$a$).

The very high magnitude of $-\rho\overline{uw}$ is also associated with the large-scale periodic structure of $w$, for locations in the rod-to-rod gap away from the duct symmetry boundary. It should be noted that the correlation functions were calculated for sufficiently long record lengths to ensure reasonable statistical accuracy, and without recourse to conditional sampling techniques (Hooper 1983; Hooper & Rehme 1983).

### 5.2. *Symmetrical square-pitch rod array*

The structural analysis of the turbulent flow in the open rod-gap region was repeated for the symmetrical square-pitch rod array ($p/d = 1.107$), at a Reynolds number of $49 \times 10^3$ corresponding to a mean axial velocity of 10.3 m s$^{-1}$. The experimental technique is described in §5.1. For this rig the turbulence intensity levels in the open rod gap were sufficiently small to allow accurate use of the hot-wire anemometer small-signal approximations (Hooper 1980$a$). The omission of spacer grids or pins from the test section ensured that there would be no wake likely to be associated with the large-scale structure of $u$ and $w$.

#### 5.2.1. *Direct reproduction of turbulent-velocity components*

The output from the two hot-wire probes, located on the $y$-axis at coordinates (0, $\pm 10.2$ mm), was processed to give the direct signal of the $u$, $v$ and $w$ turbulence components. The $(x,z)$-plane results (figure 19$a$) show large-scale, almost-periodic, fluctuations in the axial turbulence component $u$ on each side of the rod gap. The probe locations correspond to the intersection of radial traverses at $\pm 15°$ in the rod-centred cylindrical coordinate system and the central symmetry axis passing through the rod gap ($y = \hat{y}$); at these locations the axial turbulence intensity for regions remote to the rod wall reached a local maximum (figure 9). The large-scale structure of $u$ shows that a perturbation of the axial velocity, in this region of the rod gap, is the first sign of the intersubchannel momentum exchange process which becomes dominant at low $p/d$ or $w/d$ ratios. A striking feature, evident in figure 19 ($a$), is the antiphase relationship of the large-scale $u$-structure in the neighbouring subchannels. The $x$-axis turbulent-velocity component, directed essentially towards the rod walls, again has no corresponding large-scale structure (figure 19$a$).

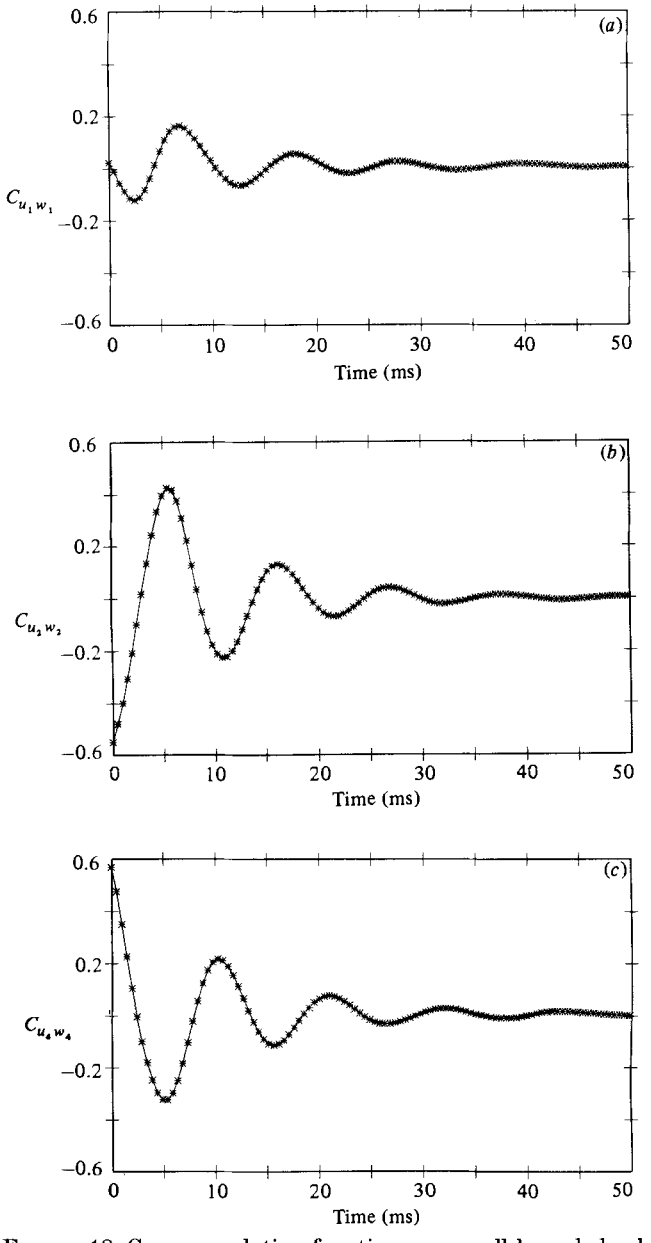


FIGURE 18. Cross-correlation function $\rho uw$; wall-bounded subchannel: (*a*) location 1; (*b*) location 2; (*c*) location 4.

Results for the $(y, z)$-plane (figure 19*b*) show that the transverse turbulent-velocity component $w$ also has large structural features, although these are considerably reduced in magnitude and without an apparent antiphase relationship.

### 5.2.2. *Spatial cross-correlation coefficients for u, v and w*

The spatial extent of the correlation between the turbulent velocity components $u$, $v$ and $w$ on either side of the $x$-axis, a subchannel boundary and rig symmetry axis which secondary-flow cells would not be expected to cross, was measured by fixing one probe at the $(x, y)$-coordinates of (0, 10.2 mm). The moving probe traversed the

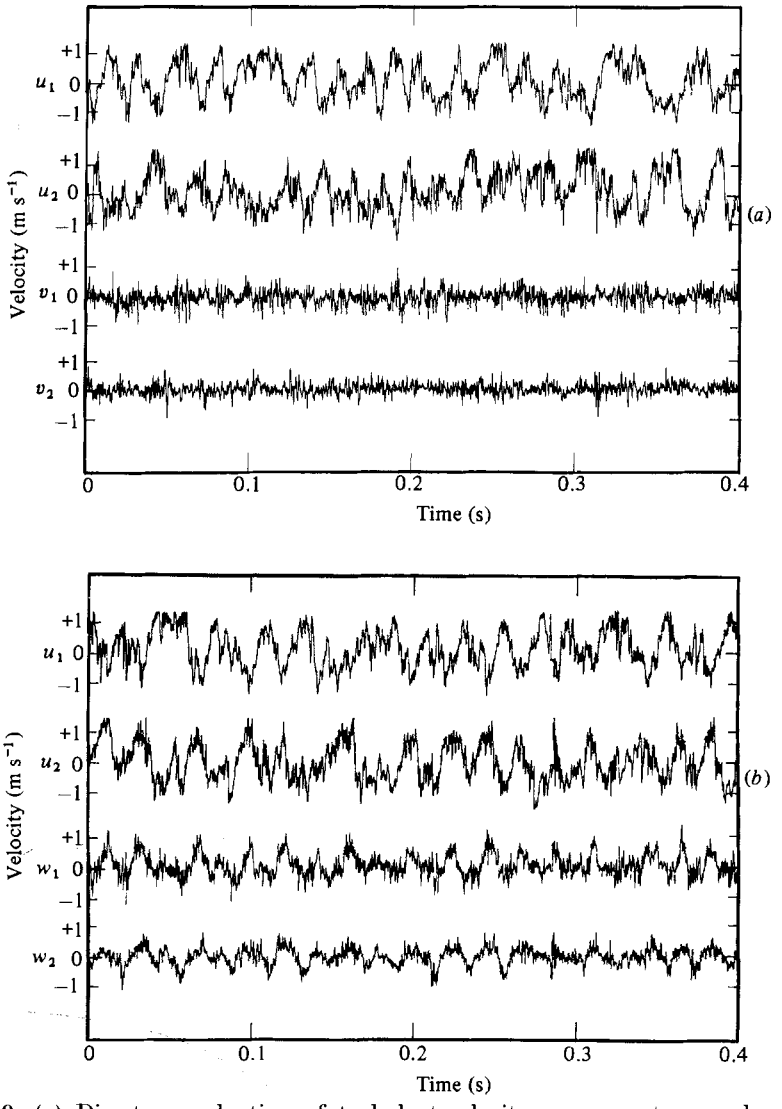


FIGURE 19. (*a*) Direct reproduction of turbulent-velocity components $u$ and $v$; symmetrical square-pitch rod array and for a Cartesian coordinate system located at the rod-gap centre ($p/d = 1.107$; $Re = 4.90 \times 10^4$). (*b*) Direct reproduction of turbulent-velocity components $u$ and $w$; symmetrical square-pitch rod array and for a Cartesian coordinate system located at the rod-gap centre ($p/d = 1.107$; $Re = 4.90 \times 10^4$).

$y$-axis, and data points were taken at locations corresponding to 0°, −5°, −10°, ..., −45° in the rod-centred cylindrical coordinates. The first data point of figure 19 is at 3°, the closest approach allowed by the traverse systems. All correlation data were calculated with a Hewlett-Packard 3721 correlator, with low-pass filtering generally at 1.5 kHz.

The spatial correlation of $u$ (shown in figure 20) is high for the majority of the traverse. The cross-correlation coefficient changes sign as soon as the subchannel boundary or $x$-axis is reached, and is effectively zero at the boundary. The maximum cross-correlation coefficient is for the $y$-axis location of the moving probe corresponding to −20° in the cylindrical coordinate system; this suggests that the most energetic

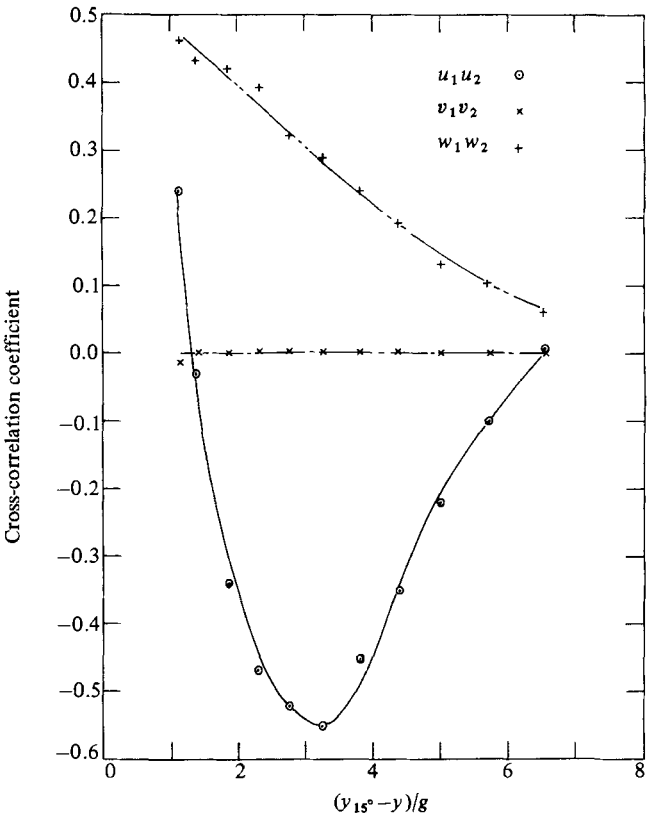


FIGURE 20. Spatial correlation of $u$, $v$ and $w$ for the rod-gap area; symmetrical square-pitch rod array ($p/d = 1.107$; $Re = 4.90 \times 10^4$).

coupling of the $u$-structure across the subchannel boundary occurs at this point and not at $\pm 15°$.

The $x$-axis turbulent-velocity component $v$ has no significant non-zero cross-correlation coefficient for all locations.

The transverse or $y$-axis turbulent-velocity component $w$ is also highly correlated through the rod gap (figure 20) over a lengthscale of at least five times the rod-gap width. There is no evidence, however, of a phase difference between the $w$-fluctuations on either side of the subchannel boundary.

### 5.2.3. *Auto- and cross-correlation functions*

The autocorrelation functions for $u$, $v$ and $w$ at $(x, y)$-coordinates (0, 10.2 mm), corresponding to ($y = \hat{y}$, $\theta = 15°$) in cylindrical coordinates, are given in figures 21(*a–c*). The axial component $u$ and transverse component $w$ both have a damped periodic response, as was the case for the wall-bounded rod array (§5.1). As expected, the $x$-axis or $v$-component has no periodic feature, even when resolved over much-reduced time steps (figure 21*b*).

The cross-correlation functions between the same turbulent-velocity components (figure 21*d–f*) are for $(x, y)$-coordinates of (0, 10.2 mm) and (0, −8.7 mm), corresponding respectively to 15° and −10° in cylindrical coordinates. The phase relationship between the large-scale structure in $u$ is 180°, with no phase change in the transverse velocity component $w$ on either side of the subchannel boundary. The

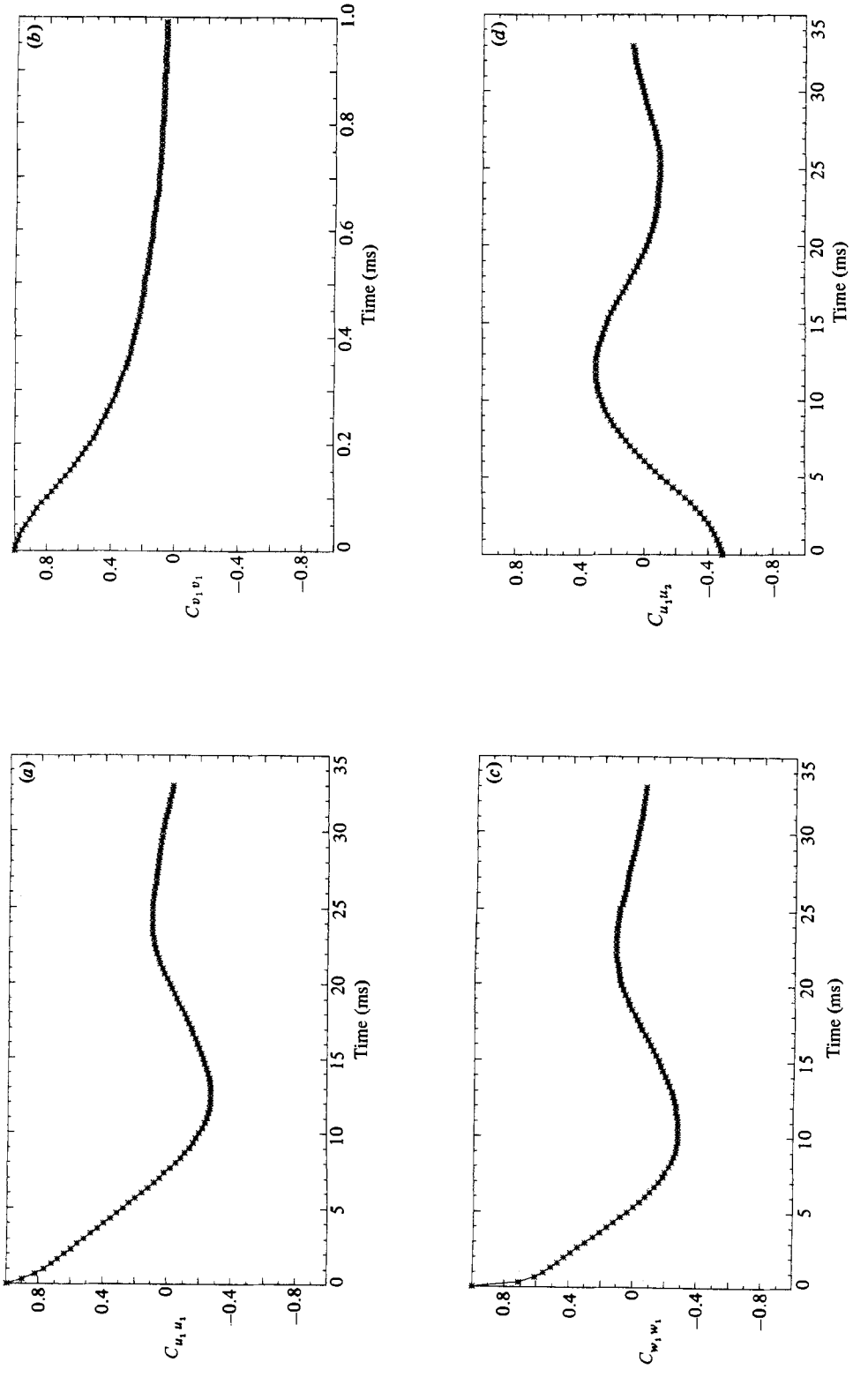
(a)
(b)
(c)
(d)
$C_{u_1u_1}$
$C_{v_1v_1}$
$C_{w_1w_1}$
$C_{u_1u_2}$
0.8
0.4
0
−0.4
−0.8
0
5
10
15
20
25
30
35
0.2
0.6
1.0
Time (ms)

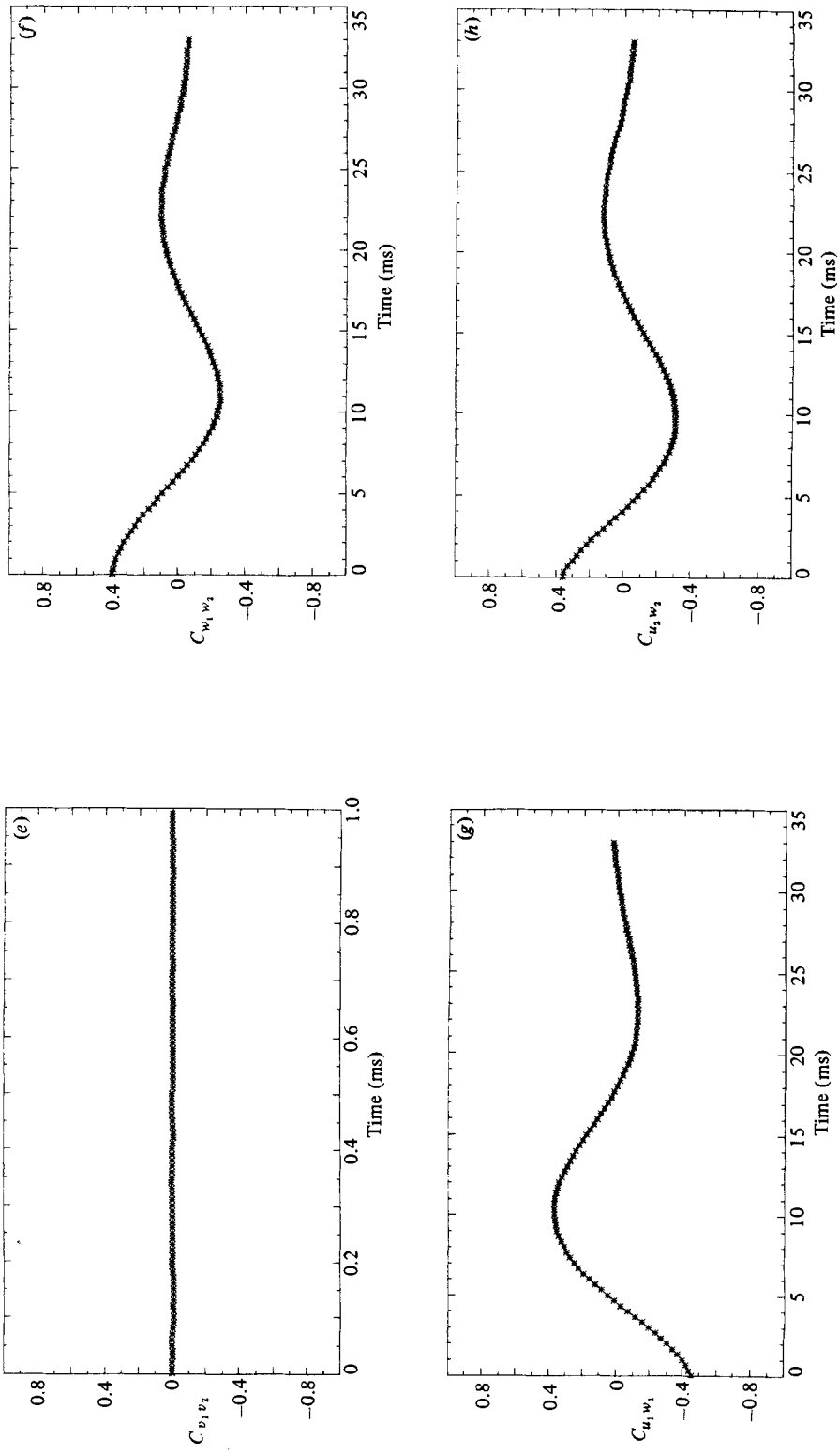


FIGURE 21. Autocorrelation functions of (*a*) $u$, location 1; (*b*) $v$, location 1; (*c*) $w$, location 1. Cross-correlation functions; (*d*) $u_1 u_2$, locations 1 and 2; (*e*) $v_1 v_2$, locations 1 and 2; (*f*) $w_1 w_2$, locations 1 and 2; (*g*) $u_1 w_1$, location 1; (*h*) $u_2 w_2$, location 2.

cross-correlation for $v$ (figure 21*e*) has no significant non-zero level, again demonstrating the very restricted lengthscale of $v$ in the rod gap.

The high levels of the azimuthal component of the Reynolds shear stress, resolved in rod-centred cylindrical coordinates (figure 11), is also associated with the large-scale structure of $u$ and $w$. The cross-correlation function for these components (figures 21*g*, *h*) show the same periodic structure as the autocorrelations, despite the corresponding 15° and −10° rotation of the Cartesian coordinates with reference to the cylindrical coordinate system. The antisymmetry of $-\rho\overline{uw}$ with respect to the subchannel boundary, in either coordinate system, is attributed to the 180° phase change in the large-scale structure of the axial component $u$.

## 6. Discussion

The development of a large-scale structure for the axial and transverse turbulent-velocity components in the rod-to-rod gap region may be viewed as typical of developed single-phase flow through closely spaced rod arrays only after the elimination of the more obvious generating mechanisms:

(i) rod vibration coupled to the fluid by the virtual-mass effect (J. J. Thompson 1982 private communication, University of N.S.W.);

(ii) vortex shedding by spacer pins in the rod gap;

(iii) impressed large-scale structure in the fluid before the test-section entry, and incomplete flow development;

(iv) acoustic resonance in the test section.

The possibility that the large-scale structure of $u$ and $w$ is excited by a mechanical rig vibration was tested experimentally by locating an accelerometer mid-distance between the spacer pins of the Rehme (1982*c*) test section, and attaching it internally to one rod wall, opposite the rod gap. The mechanical vibrations had an r.m.s. level of approximately $0.02g$ ($g$ being the gravitational acceleration), and were uncorrelated with any of the turbulent-velocity components. Similar measurements of the rig vibration and the three turbulent-velocity components in the symmetrical square-pitch rod cluster also showed no non-zero cross-correlation, thus eliminating rig vibration as the generating mechanism.

The general features of the large-scale turbulent structure in the rod gap are similar for both test-section geometries. It is therefore probable that the 2 mm diameter spacer pins, used in the wall-bounded rod array to maintain the geometrical accuracy of the test section, have a negligible effect on this structure. The independence of the Reynolds-stress distribution to the rig entry conditions for the symmetrical square-pitch rod array is an indication that the flow is developed, and that structural effects are independent of flow structure generated externally to the test section.

The possibility that an acoustic resonance effect is the generating mechanism in the test section was suggested by P. Bradshaw (1982 private communication, Department of Aeronautics, Imperial College, London); this may best be discounted by demonstrating the dependence of the effective structural frequency on the Reynolds number. An acoustic resonance phenomenon would be of fixed frequency for a fixed test-section length. The Reynolds-number dependence of the effective or time-averaged frequency of the large-scale structure of the rod-gap turbulence, over an approximate 10:1 range, is shown in figure 22. One-quarter of the time-averaged period was taken to be the time to the first zero of the autocorrelation function of $u$, and the near-linear relationship shows that the Strouhal number of the structure is independent of Reynolds number.

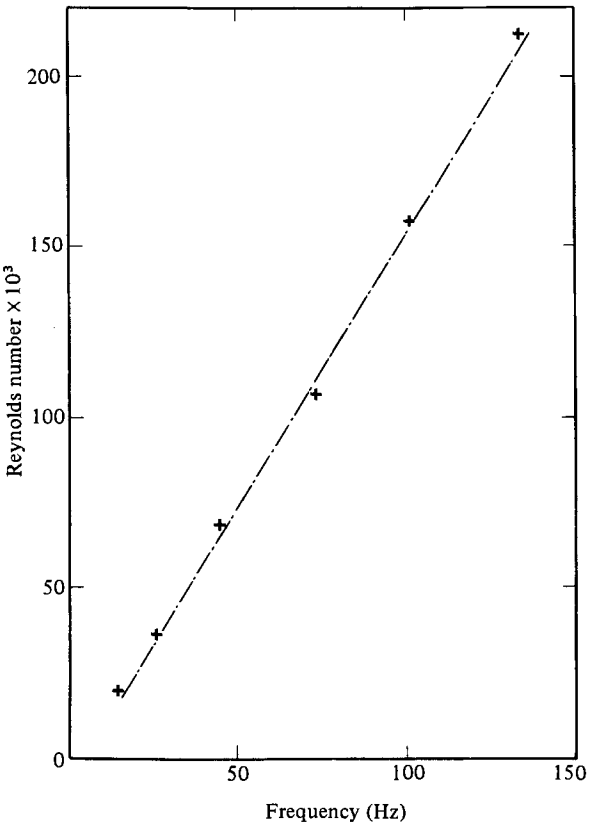


FIGURE 22. Mean cyclic frequency of large-scale turbulent structure in the open rod gap of the symmetrical square-pitch rod subchannel ($p/d = 1.107$) as a function of Reynolds number.

Perhaps the strongest evidence for an incompressible-flow intersubchannel instability as the generating mechanism, suggested initially by Bradshaw (1982 private communication), is the 180° phase relationship between the large-scale structure of the axial turbulent-velocity component with respect to the subchannel boundary. If the mass flow in one subchannel decreases, the local axial pressure gradient also decreases, with the generation of a transverse pressure difference between it and the adjacent subchannel. For low $p/d$ or $w/d$ ratios phase lags between turbulent velocity components $u$ and $w$, and the local intersubchannel static pressure fluctuation apparently make this an unstable situation. It is not possible to measure the spatial gradient of this pressure fluctuation, despite the very high levels reached by the Reynolds-stress components $-\rho\overline{u^2}$, $-\rho\overline{w^2}$ and $-\rho\overline{uw}$, which indicates that the pressure fluctuation is at least of comparable magnitude to the mean axial static pressure gradient.

The intersubchannel instability perturbs the axial turbulent-velocity component $u$ most energetically well away from the rod walls, in the area defined by a rod-centred cylindrical coordinate system for traverses between $\pm 15°$ and $\pm 20°$, and for wall distances approximately equal to $\hat{y}$. As the rod gap width is reduced, the increasing magnitude of the pressure-driven intersubchannel instability is shown by the selective amplification or excitation of the $-\rho\overline{u^2}$, $-\rho\overline{w^2}$ and $-\rho\overline{uw}$ Reynolds-stress components.

The possibility of coupling between the fluid structures in adjacent rod gaps,

indicated by the Reynolds-stress distribution for the wall-bounded rod array, is supported by the lengthscales demonstrated for $u$ and $w$. The symmetrical square-pitch rod array, with a single open rod gap, may, however, overestimate the spatial correlation lengths of $u$ and $w$.

## 7. Conclusions

Mass-, momentum- and heat-transfer processes in the rod-gap area for developed single-phase turbulent flow through closely spaced rod arrays are governed by an energetic and almost periodic azimuthal turbulent-velocity component directed through the rod gap. The azimuthal turbulent-velocity component is not associated with mean secondary-flow velocities driven by Reynolds-stress gradients, but apparently generated by an incompressible-flow parallel-channel instability. The axial turbulent-velocity component develops a corresponding large-scale structure which is highly correlated through the rod gap, but has an 180° phase difference on either side of the subchannel boundary. In symmetrical arrays, the most energetic perturbation to the axial velocity component occurs in the central gap area for radial traverses between $\pm 15°$ and $\pm 20°$, relative to the subchannel and symmetry boundary at 0°. There is evidence of instability for rod spacings down to a lower limit of 1.026 ($p/d$ or $w/d$ ratio), which may be dependent on Reynolds number. The long lengthscales of the axial and azimuthal turbulent-velocity components, relative to the gap width, emphasize the anisotropy of the turbulent transport processes in the rod gap, an important feature to reproduce in numerical models of rod-bundle flow.

The experimental work for studies on the wall-bounded rod array was performed by Messrs E. Mensinger and G. Wörner of the KfK Karlsruhe, Federal Republic of Germany. The symmetrical square-pitch array was constructed by Mr W. J. Crawford of the Australian Atomic Energy Commission, who also provided experimental assistance and constructed the hot-wire probes. This project was carried out at the Lucas Heights Research Laboratories and supported by the Australian Atomic Energy Commission.

## REFERENCES

ALY, A. M. M., TRUPP, A. C. & GERRARD, A. D. 1978 *J. Fluid Mech.* **85**, 57.

BRUNDRETT, E. & BAINES, W. 1964 *J. Fluid Mech.* **19**, 375.

BRUUN, H. 1976 *J. Fluid Mech.* **76**, 145.

CARAJILESCOV, P. & TODREAS, N. E. 1976 *Trans. ASME* C: *J. Heat Transfer* **98**, 262.

CHAMPAGNE, F. H. & SLEICHER, C. A. 1967 *J. Fluid Mech.* **28**, 177.

EIFLER, W. & NIJSING, R. 1973 *Rep.* EUR-4950 e.

GALBRAITH, K. P. & KNUDSEN, I. G. 1972 *Am. Inst. Chem. Engng* **68**, 90.

GESSNER, F. B. 1973 *J. Fluid Mech.* **58**, 1.

HAQUE, M. A., HASSAN, A. K. A., TURNER, J. T. & BARROW, H. 1983 *Wärme und Stoffübertragung* **17**, 93.

HOOPER, J. D. 1980*a* Fully developed turbulent flow through a rod cluster. Ph.D. thesis, University of N.S.W.

HOOPER, J. D. 1980*b* *Nucl. Engng Des.* **60**, 365.

HOOPER, J. D. 1983 In *Proc. 4th Symp. Turbulent Shear Flows, Karlsruhe.*

HOOPER, J. D., WOOD, D. H. & CRAWFORD, W. J. 1983 *AAEC Rep.* E558.

HOOPER, J. D. & REHME, K. 1983 *KfK Rep.* 3467.

KJELLSTRÖM, B. 1974 *AB Atomenergi Rep.* A.E.-487.

LAUFER, J. 1954 *NACA Rep.* 1174.
LAUNDER, B. E. & YING, Y. M. 1972 *J. Fluid Mech.* **54**, 289.
LAWN, C. J. 1971 *J. Fluid Mech.* **48**, 477.
MELLING, A. & WHITELAW, J. H. 1976 *J. Fluid Mech.* **78**, 289.
PATEL, V. C. 1965 *J. Fluid Mech.* **23**, 185.
PERKINS, H. J. 1970 *J. Fluid Mech.* **44**, 721.
REHME, K. 1977 *KfK Rep.* 2441 [English Transl. *W.H. Trans.* 404 (1977)].
REHME, K. 1978*a* *KfK Rep.* 2617.
REHME, K. 1978*b* *KfK Rep.* 2637.
REHME, K. 1980*a* *KfK Rep.* 2983.
REHME, K. 1980*b* *KfK Rep.* 3047.
REHME, K. 1980*c* *KfK Rep.* 3069.
REHME, K. 1981 *IAHR Conf. Paper, MIT.*
REHME, K. 1982*a* *KfK Rep.* 3318.
REHME, K. 1982*b* *KfK Rep.* 3324.
REHME, K. 1982*c* *KfK Rep.* 3361.
REHME, K. 1982*d* *Nucl. Technol.* **59**, 148.
ROWE, D. S. 1973 *BNWL Rep.* 1736.
SEALE, W. J. 1979 *Nucl. Engng Des.* **54**, 183.
SEALE, W. J. 1982 *J. Fluid Mech.* **123**, 399.
TRUPP, A. C. & AZAD, R. S. 1975 *Nucl. Engng Des.* **32**, 47.
WOOD, D. H. 1981 *Univ. Newcastle (Australia) Rep.* TN-FM61.
WOOD, D. H. & HOOPER, J. D. 1984 *Nucl. Engng Des.* (to appear).